Probabilistic Injury Risk Function Development for the liver, spleen, and small intestine of the 50th percentile male THUMS version 7 finite element model

Florent Auriault, Pascal Baudrit, Matthieu Lebarbé, Marko Cvetković, Mitsutoshi Masuda

Abstract Finite Element Human Body Models (HBMs) are powerful tools dedicated to analyzing the human body's response to injuries when subjected to dynamic loading, such as occurs in Motor Vehicle Crashes. In order to predict injuries, these models need to be associated with relevant injury criteria. In this study, simulation-based Injury Risk Functions (IRF) of the abdominal organs were developed using the 50th percentile Male (M50) Total Human Model for Safety version 7 (THUMS v7). A total of 14 studies reporting laboratory test series on post-mortem human subjects (PMHS) were collected from the literature to be replicated with the M50 THUMS v7 model. A closer review of each PMHS test was performed to exclude the non-usable ones. Finally, 177 PMHS tests were included in this analysis to develop the IRFs. The experiments were replicated with the HBM, and different mechanical metrics were extracted from the liver, spleen, and small intestine elements. IRFs were developed using a survival analysis, following the principles of ISO Technical Specifications 18506 (2014). As a last step, the ability to predict abdominal injuries using the model and the newly developed IRFs was assessed using one additional PMHS test series.

Keywords Injury risk function, human body model, abdominal organ tolerances, finite element simulations, THUMS.

I. INTRODUCTION

The abdominal organs are frequently injured in Motor Vehicle Crashes MVCs [1-2]. In frontal MVCs, the most frequently injured abdominal organs are the spleen, the jejunum, and the liver [3]. The occurrence of injuries in these organs may increase with the use of reclined posture. In the literature, abdominal injury tolerances have been studied based on Post-Mortem Human Subjects (PMHS) experiments [4-5], and Injury Risk Functions (IRFs) have been developed for Anthropomorphic Test Devices (ATDs) [6] and Human Body Models (HBMs) [7]. Compared to ATDs, HBMs are powerful tools as they can be used in complex loading scenarios which allow analysis of the injury outcomes to improve safety in such scenarios. The use of these models is increasing in the field of passive safety and the European New Car Assessment Programme (Euro NCAP) will include virtual testing with occupant HBM in its vehicles rating protocol in the coming years. Consequently, there is a need to improve the HBMs' ability to predict injuries. Beillas *et al*. [7] developed IRFs for the liver and the spleen for two models of the Global Human Body Model Consortium (GHBMC): the detailed small female and the detailed mid-size male. The IRFs were based on the Strain Energy Density of the organ as injury criterion. However, these curves are specifics to the GHBMC models and cannot be directly used with other HBMs, such as the 50th percentile Male Total Human Model for Safety version 7 (M50 THUMS v7) [8].

The M50 THUMS version 7 model is a detailed Finite Element (FE) human model validated against a wide range of PMHS test responses. Each body region of the model was validated using a total of 38 configurations described in the THUMS model user manual. Among these, seven concern the abdomen (directly or indirectly) in frontal and lateral impact configurations. The response in a reclined seating posture in frontal impact has already been addressed [8]. However, to make it more relevant for the analysis of MVCs, the model should be associated with IRFs for the different body regions. While extensive work has already been carried out regarding the head [9] and thorax [10-11], there is a lack of injury criteria for the abdominal organs of the model. This gap is addressed by the present study, which developed simulation-based IRFs specific to the M50 THUMS v7 model for the prediction of liver, spleen or Small Intestine (SI) injuries. The chosen injury severity level is AIS2+ [12].

F. Auriault (e-mail: florent.auriault@ceesar.fr) is a Researcher and P. Baudrit and M. Lebarbé are Senior Researchers at CEESAR, France. M. Cvetković is a Senior Researcher at Toyota Motor Europe, Belgium. M. Masuda is a Senior Researcher at Toyota Motor Corporation, Japan.

II. METHODS

To develop the abdominal organs' simulation-based and model-specific IRFs, four main steps were defined: (I) a literature review was conducted to identify experimental tests on PMHS reporting both the different abdominal organ injury outcomes and well described boundary conditions; (II) tests were replicated with M50 THUMS v7 and local mechanical metrics were extracted from the abdominal organs; (III) pairing the HBM metrics with the PMHS injury outcomes, IRFs were developed using a survival analysis; (IV) the injury probability predicted by the model was compared to the real injury risk of PMHS with an additional impact configuration – a far-side sled.

Source data

The literature review was searched for studies focusing on PMHS abdominal response and injuries under impact. The collected data covered abdomen-specific tests or full-body tests for which boundary conditions were sufficiently documented to enable their replication by numerical simulations. The literature review could also include unpublished tests. Of course, the THUMS v7 validation cases were included. Eventually, a total of 14 studies were gathered in this analysis, leading to 177 experiments with 145 PMHS. An overview of the studies is presented in Table I. All the loading configurations are shown in detail in Appendix AI and Tables AI to AV, with drawings, PMHS information, and a synthetic description of boundary conditions used in the simulations. Excluded studies and subjects are presented in Table AVI.

TABLE I
EXPERIMENTAL CONFIGURATIONS AND SIMULATIONS OVERVIEW

	Configuration type	1st Author	Number of PMHS
Frontal loading	Impactor tests at L3 or T11 level	Hardy [13]	12
	18 kg rigid rim impact at L3	Nusholtz [14]	3
	63 kg or 31 kg rigid bar impact at L1 or L3	Cavanaugh [15]	11
	Belt pull on soft abdomen	Trosseille [16]	6
		Lamielle [17]	8
		Hardy [13]	3
		Foster [18]	8
		Ramachandra [5]	7
	3-pt belt loading (upright or inverted)	Howes [19]	6
Lateral loading	23 kg impactor, oblique or lateral	Viano [20]	14
	Right lateral or oblique impact	Kremer [21]	10
	Right drop test with offset	Walfisch [22]	4
	Lateral sled test	Cavanaugh [23]	14
	Lateral sled test	Maltese [24]	39

Computational Modelling

The different experimental tests were replicated with M50 THUMS v.7 model in the LS-DYNA environment (ANSYS/LST, Livermore, CA). The simulations were started with version R11.2.2 of the solver on single precision and with 32 CPUs. In the simulations, boundary conditions were defined to match those of the PMHS tests and scaled when necessary to take into account the mass difference between the subjects and the HBM.

Free flight impactor configurations: for these configurations, an initial velocity was imposed on the impactor coming into contact with the HBM. Depending on the configurations, the HBM was or was not in a free back configuration and the impact angle/location was defined to match the experimental test conditions. The initial velocity (V_0) of the impactor was scaled according to the different masses (m) involved using Eq. (1) [25]:

$$V_{0\_HBM} = V_{0\_PMHS} * \sqrt{\frac{m_{HBM}+m_{impactor}}{m_{PMHS}+m_{impactor}}} \quad (1)$$

Abdominal belt loading configurations: for these configurations, the experimental force time history curves were scaled and applied directly on the belt extremities. Equal-stress/equal-velocity scaling [26] was used to scale the curves, as proposed in Foster *et al*. [18] (Eqs (2)–(4)). In accordance with test configurations, the HBM was or was not in free back condition, with a position similar to the one from the experiments:

$$F_{HBM} = \lambda^{\frac{2}{3}} F_i \mathrm{d} \quad (2)$$

$$T_{HBM} = \lambda^{\frac{1}{3}} T_i \quad (3)$$

$$\lambda = \frac{m_{HBM}}{m_i} \quad (4)$$

with F being the force, T the time, m the mass, and λ the body mass ratio; suffix "i" stands for the considered PMHS case, and suffix "HBM" stands for THUMS model.

Drop tests configurations: rather than replicating drop tests with the HBM, the scaled force versus time response curve coming from the experiments was applied as an imposed force on the impacting surface. Only configurations with a rigid armrest were replicated and the experimental forces were scaled using the equal-stress/equal-velocity scaling (Eqs (2)–(4)).

Lateral sled configurations: no scaling was used and only one simulation was performed for each condition. The HBM was seated on the sled as in the experiments. An initial velocity was imposed on the HBM to reproduce the loading.

For the same configuration with variations in boundary conditions between different tests (for example, the impactor initial velocity), not all tests were replicated in order to reduce the total number of simulations and the computational time. However, all the PMHS cases of the same configuration could be used by performing a linear or polynomial regression between the HBM output metrics (for example, the maximum strain of an element as a function of the impactor initial velocity on the simulated cases). Thus, the metric values of the non-simulated experiments were interpolated from the regression. Typical examples of regression are presented in Fig. 1. Eventually, a total of 94 simulations were run for a total of 177 experiments. Table II presents the different loading cases, the number of physical tests used in this study, and the number of simulations and interpolated data performed for the analysis.

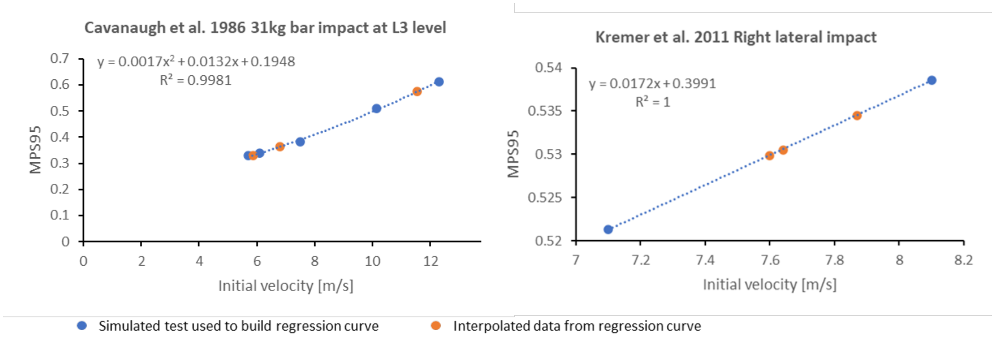

Fig. 1. Regression example

IRF development

Based on the selected dataset, and due to the limited data related to injuries on the stomach and kidneys, it was not possible to develop an IRF for these organs. Only the liver, spleen and Small Intestine (SI) were considered for IRFs development. The IRFs were computed using a survival analysis, following the principles of ISO Technical Specifications 18506 (2014), also reported in Petitjean *et al*. [27], and with The R software.

Censoring status. The data were censored as follows:

- Left censored if the PMHS was used only once and the organ was injured.

- Right censored if the PMHS was used only once and the organ was not injured.
- Right censored if the same PMHS was used several times and the organ was not injured. The simulation providing the highest metric value was considered.
- Interval censored if the same PMHS was impacted several times and the organ was injured. In that case, and for the interval definition, the simulations with the lowest and the highest metric values were considered.

Metric selection. Different metrics were considered as potential injury predictors at the elements level. These metrics are presented in Table III. For the solid organs (liver and spleen), the metrics were extracted from solid elements of the corresponding parts, while they were extracted on 2D elements (corresponding to the external surface of the organ) for the small intestine (hollow organ). The solid parts of the liver and spleen are both modelled with a rubber material model (Mat 181 from the lsdyna library). The surface of the small intestine is modelled with a fabric material (Mat 034 of the lsdyna library). Regarding the latter, only the ileum and the jejunum were considered to extract metrics as the duodenum was modelized with different material properties in the THUMS v7 model. The Area under the Receiver-Operating Characteristic curve (AROC) was used to select the most appropriate metric [27]. The AROC is a value between 0 and 1 telling how well the metric explains the injury occurrence. In our study, the metrics with the highest AROC values over 0.5 were considered to build the the IRF.

Distribution law selection. Three parametric statistical distributions were used for the analysis: Weibull, Log-Normal and Log-Logistic. The Akaike Information Criterion (AIC) was computed to select the best distribution. The distribution with the lowest AIC value should be selected (if the difference of AIC is greater than 2). The parametric IRFs were superimposed with the non-parametric IRFs to visually check the distribution assumption.

IRF Quality Index. Finally, as proposed in ISO TS 18506 (2014), a Quality Index (QI) of the curve was computed: the relative size of the confidence interval for 5%, 25% and 50% of risk. A QI lower than 0.5 is considered a good rating, between 0.5 and 1 a fair rating, between 1 and 1.5 a marginal rating, and an unacceptable rating if greater than 1.5 [27].

In addition, following the methodology proposed by Beillas *et al.* [7], two datasets (referred as "groups") were used to build IRFs. Group 1 contained all the loading cases considered in this study (full dataset). Group 2 was a sub-sample of the dataset, gathering only the experiments for which an actual loading of the considered organs was known. Concisely, the following experimental tests were excluded from group 2 (see Table II): bar impacts at the abdominal area and abdominal loading with lap belt. The amount of data for each organ and their censoring using group 1 and group 2 are presented in Table IV. IRFs were then developed using group 1 and group 2 for the liver and spleen, but only group 1 was used for the SI, considering it filled the whole abdominal cavity and was then loaded in each configuration.

TABLE II

EXPERIMENTAL CONFIGURATIONS AND SIMULATIONS OVERVIEW

Ref.	Loading case	Number of tests	Number of simulations	Number of interp. data	Number of injurious cases (AIS2+)			Used in group 2
					Liver	Spleen	SI	
[15]	Frontal impact bar 31 kg at L3	7	5	2	0	0	0	No
[15]	Frontal impact bar 63 kg at L3	3	2	1	0	0	0	No
[15]	Frontal impact bar 63 kg at L1	1	1	0	1	1	0	No
[13]	Airbag surrogate	6	3	3	2	0	0	No
[13]	Frontal impact bar 48 kg at L3	6	4	2	5	2	0	No
[13]	Frontal impact bar 48 kg at T11	3	2	1	3	1	0	No
[14]	Frontal impact 18 kg "steering wheel"	13	5	5	2	0	0	No
[21]	Right lateral impactor at abdomen	5	2	3	2	0	0	Yes
[21]	Right oblique impactor at abdomen	5	2	3	5	0	0	Yes
[20]	Left lateral impactor at Xiphoïd	2	2	0	0	0	0	Yes
[20]	Left or right oblique impactor at Xiphoïd or Abdomen (multiple impacts)	28	15	13	2	1	0	Yes

TABLE II
EXPERIMENTAL CONFIGURATIONS AND SIMULATIONS OVERVIEW

Ref.	Loading case	Number of tests	Number of simulations	Number of interp. data	Number of injurious cases (AIS2+) Liver	Spleen	SI	Used in group 2
[13]	Belt on soft abdomen	3	3	0	0	0	0	No
[16]	Belt on soft abdomen	6	6	6	1	1	1	No
[17]	Belt on soft abdomen	8	8	0	2	3	7	No
[5]	Belt on soft abdomen	10	6	4	0	1	1	No
[18]	Belt on soft abdomen	8	8	0	3	1	0	No
[19]	3-pt belt loading	6	6	0	3	0	5	No
[22]	Drop tests	4	3	1	3	0	0	Yes
[23]	Left sled RxF	5	1	0	0	2	0	Yes
[23]	Left sled Psoft	5	2	0	0	0	0	Yes
[23]	Left sled Pstiff	4	1	0	0	2	0	Yes
[24]	Left sled RxF	18	2	0	5	5	0	Yes
[24]	Left sled PxF	14	2	0	5	5	0	Yes
[24]	Left sled RxOT	4	1	0	0	0	0	Yes
[24]	Left sled RxOA	2	1	0	0	0	0	Yes
[24]	Left sled RxOP	1	1	0	0	0	0	Yes

Note: *R*F = Rigid flat wall; R*Psoft - Soft padded wall; Pstiff = Stiff padded wall; P*F = Padded Wall; R*OT = Rigid wall offset on Thorax; R*OA = Rigid wall offset abdomen; R*OP = Rigid wall offset pelvis.*

TABLE III
METRICS OVERVIEW

Potential predictor	Metric
Maximal Principal Strain (true) (MPS)	Peak, 95th and 90th percentile
Minimal Principal Strain (true) (MinPS)	Peak, 95th and 90th percentile
First Principal Strain (Green St Venant) (FPS)	Peak, 95th and 90th percentile
Third Principal Strain (Green St Venant) (TPS)	Peak, 95th and 90th percentile
Strain Energy Density (SED)	Peak, 95th and 90th percentile
Pressure (Press) (Small intestine)	Peak, 95th and 90th percentile

TABLE IV
AMOUNT OF DATA IN EACH GROUP, WITH CENSORING STATUS

	Group 1				Group 2			
Organ	right censored	left censored	Interval censored	Total	right censored	left censored	Interval censored	Total
Liver	101	39	5	145	59	23	2	84
Spleen	120	24	1	145	68	15	1	84
SI	131	13	1	145	Not relevant			

IRFs evaluation

As a last step, the injury prognoses predicted by the newly developed IRFs was checked using an additional test series (N=6) from the literature, replicated with THUMS. The test configuration is the sled lateral impact from Petit *et al*. [28] with the subjects in far-side condition. Each of the 6 PMHS were tested once, all with the same boundary conditions. Reference injury probabilities were computed for each organ by counting the injurious tests over the total 6 tests. These probability figures were compared with the injury risk from the simulation, computed using the metrics output values and the IRFs.

The test configuration from Petit *et al.* [28] were developed to replicate a far-side impact with a simplified sled environment (Fig. 2). The test set-up consisted of a rigid seat, a rigid seatback equipped with a headrest, a rigid footrest, and a horizontal hand support at the level of a steering wheel. Two rigid panels covered with 50 mm foam were installed at the right of subject: one representing a central console and covering the pelvis and the abdomen areas; and another one covering the whole lower limbs. The specimens were installed on the seat and belted with a 3-point seat belt. The hands and feet were free to move laterally on their supports. Finally, a lateral pulse (corresponding to a Delta-V of 8 m/s) was applied to the sled from the right to the left, so that the subjects were impacted on their right side by the central padded panels.

To reproduce these experiments, the HBM was seated in the sled environment with a position similar to that of the PMHS and the experimental pulse was applied on the sled.

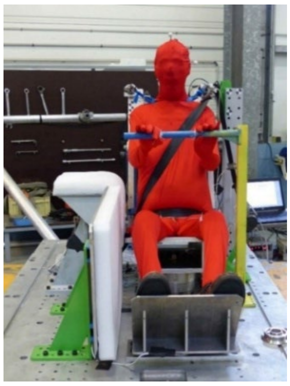

Fig. 2. Far-side configuration from Petit *et al.* [28].

Table V provides the Petit *et al.* [28] test matrix, with subjects' characteristics and abdominal injuries outcomes. Over 6 PMHS tests, one subject sustained a liver injury and another one a splenic injury. None of the subjects sustained intestinal injury. Thus, the probability of having an injury was estimated to 17% both for the liver and the spleen, and 0% for the SI, in the Petit *et al.* test configuration.

TABLE V
PMHS INFORMATION AND INJURY OUTCOME [28]

Specimen	**Test number**	**Age (yrs)**	**Sex**	**Liver injury**	**Spleen injury**	**SI injury**
736	FARSIDE 3	74	M	No injury	No injury	No injury
737	FARSIDE 4	82	M	No injury	No injury	No injury
738	FARSIDE 5	88	M	AIS2	No injury	No injury
739	FARSIDE 9	73	M	No injury	No injury	No injury
740	FARSIDE 10	87	M	No injury	AIS2	No injury
741	FARSIDE 11	91	M	No injury	No injury	No injury
Estimated probability of injury				17%	17%	0%

III. RESULTS

Before the extraction of the metrics and the generation of the IRFs, the biofidelity of the model was assessed for each configuration with a comparison of the model response vs. PMHS responses. This was mainly done in terms of force vs. deflection responses. The model was already validated regarding all the configurations coming from the THUMS v7 validation catalogue and the model responses were in accordance with the experimental responses for the other loading cases.

Liver AIS2+ IRF

The best predictor according to the AROC values was the 95th percentile of the first principal strain (FPS95) (AROC value: 0.691) for group 1 sample, and the 95th percentile of the Maximal Principal Strain (MPS95) (AROC value: 0.787) for group 2 sample, respectively (Fig. 3 and Fig. 4). However, to facilitate the IRF comparison between group 1 and group 2, it was decided to present the results for group 1 using the MPS95 (AROC value: 0.682, note this value is very close to the one for the FPS95). For both groups, the lowest AIC value was reached using a Weibull distribution (Eq. (5)). The IRFs are presented in Fig. 5 and Fig. 6. The parametric IRFs are compared to the non-parametric IRFs in Fig. 7 and Fig. 8. The quality index is presented in Table VI. The IRFs computed with group

2 presented the best QI scores for all evaluated risks: 5%, 25%, and 50%, with the rating as “good”.

$$P(Injury) = 1 - e^{-(\frac{MPS95}{\lambda})^{\gamma}} \quad (5)$$

with λ being the scale parameter and γ being the shape parameter.

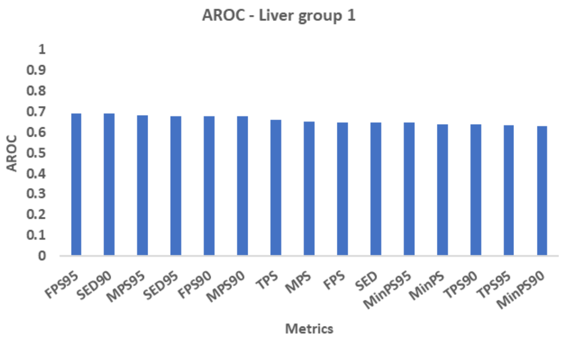

Fig. 3. AROC values for the liver using group 1.

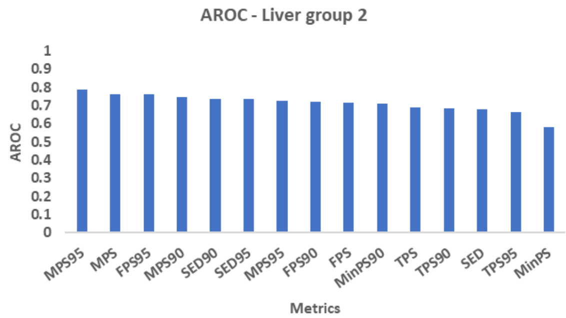

Fig. 4. AROC values for the liver using group 2.

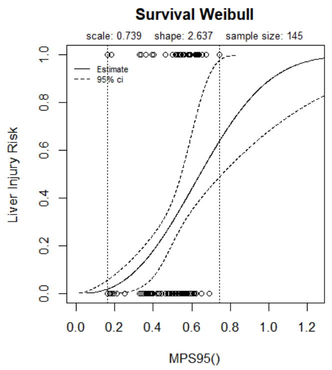

Fig. 5. Liver IRF for the group 1 using MPS95 and a Weibull distribution.

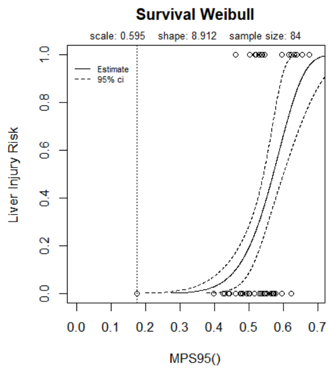

Fig. 6. Liver IRF for the group 2 using MPS95 and a Weibull distribution.

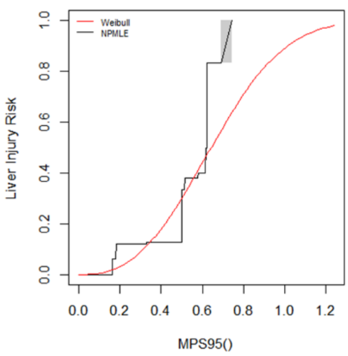

Fig. 7. Liver parametric IRFs and non-parametric IRFs for group 1.

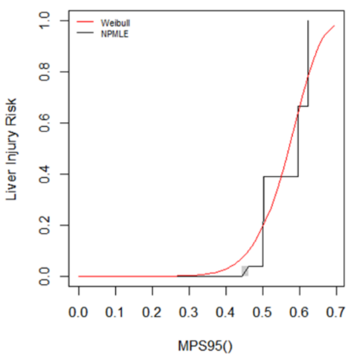

Fig. 8. Liver parametric IRFs and non-parametric IRFs for group 2.

TABLE VI
LIVER IRF QI (GOOD IN GREEN, FAIR IN YELLOW)

	Group 1			Group 2		
Predictor	QI at 5%	QI at 25%	QI at 50%	QI at 5%	QI at 25%	QI at 50%
MPS95	0.938	0.2664	0.330	0.247	0.106	0.100

Reminder for rating associated with QI values: lower than 0.5: good; between 0.5 and 1: fair; between 1 and 1.5: marginal; greater than 1.5: unacceptable.

Spleen AIS2+ IRF

The best predictor according to the AROC values was the MPS95 for both group 1 and group 2 datasets (AROC value of 0.701 and 0.759, respectively) (Fig. 9 and Fig. 10). For both groups, the lowest AIC value was reached using a Weibull distribution (Eq. (5)). The IRFs are presented in Fig. 11 and Fig. 12. The parametric IRFs are compared to the non-parametric IRFs in Fig. 13 and Fig. 14. The QI is presented in Table VII. The IRFs computed with group 2 presented the best QI scores for all evaluated risks with the rating as “fair” at 5% of risk, and “good” at 25% and 50% of risk.

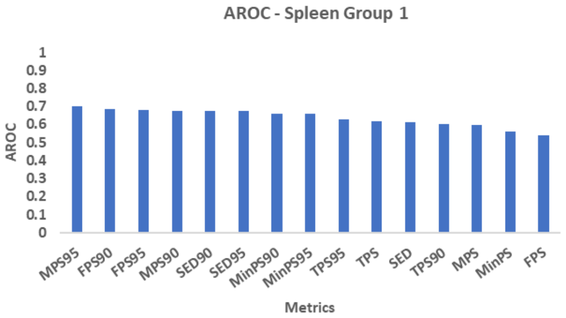

Fig. 9. AROC values for the spleen using group 1.

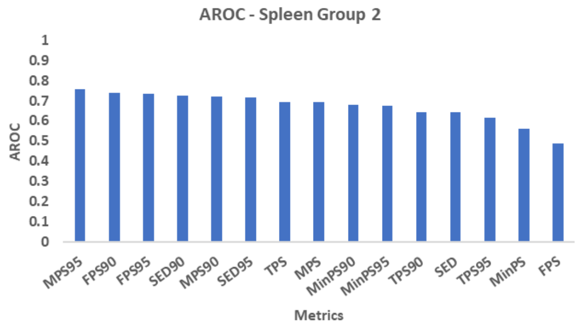

Fig. 10. AROC values for the spleen using group 2.

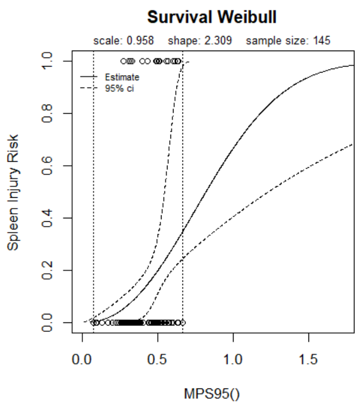

Fig. 11. Spleen IRF for group 1 using MPS95 and a Weibull distribution.

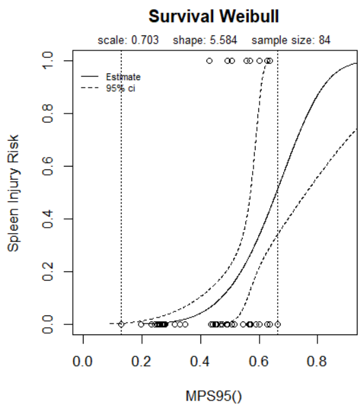

Fig. 12. Spleen IRF for group 2 using MPS95 and a Weibull distribution.

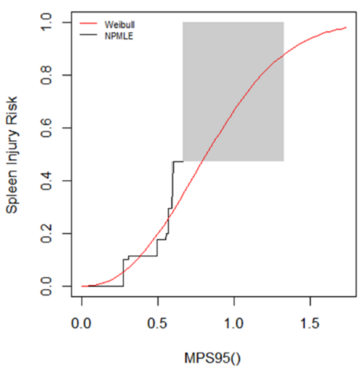

Fig. 13. Spleen parametric IRF and non-parametric IRFs for group 1.

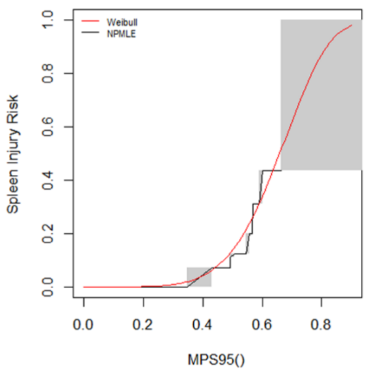

Fig. 14. Spleen parametric IRFs and non-parametric IRFs for group 2.

TABLE VII
SPLEEN IRF QI (GOOD IN GREEN, FAIR IN YELLOW, MARGINAL IN ORANGE)

	Group 1			Group 2		
Predictor	QI at 5%	QI at 25%	QI at 50%	QI at 5%	QI at 25%	QI at 50%
MPS95	1.084	0.379	0.842	0.543	0.177	0.289

Small intestine AIS2+ IRF

For the small intestine, the highest AROC value (0.789) was reached with the 95th percentile of maximal pressure extracted on the shell elements (Fig. 15). The lowest AIC value was reached using a Log-Normal distribution (Eq. (6)). The IRF is presented in Fig. 16. The comparison of the parametric IRF to the non-parametric IRF is presented in Fig. 17 and the QI in Table VIII. The rating is "good" at 5% and 25% of risk, and "fair" at 50% of risk. The confidence intervals are very wide, beyond 50% of risk, due to the absence of data.

$$P(Injury) = \phi(\frac{\ln(Press95)-\mu}{\sigma}) \quad (6)$$

with ϕ being the cumulative distribution function of the standard normal distribution, i.e. N(0,1), μ being the mean log parameter, and σ being sd log parameter.

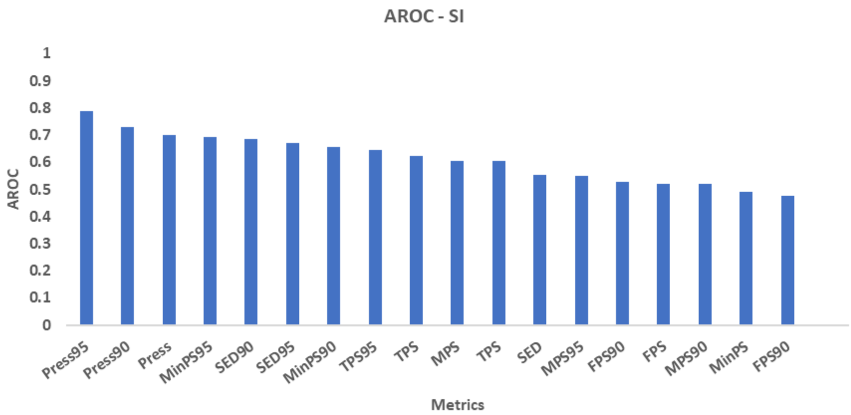

Fig. 15. AROC values for the SI.

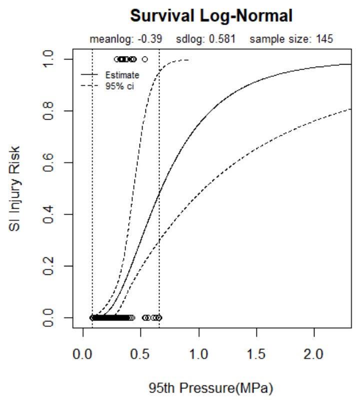

Fig. 16. SI IRF: the 95th percentile of pressure with a lognormal distribution.

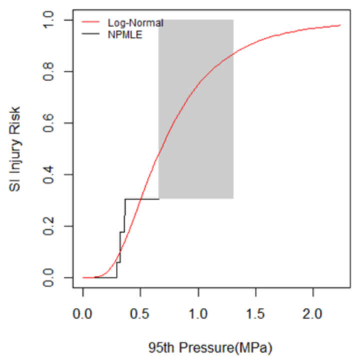

Fig. 17. SI parametric IRFs and non-parametric IRFs.

TABLE VIII
SMALL INTESTINE IRF QI (GOOD IN GREEN, FAIR IN YELLOW, MARGINAL IN ORANGE)

	Group 1		
Predictor	QI at 5%	QI at 25%	QI at 50%
95th percentile maximal pressure	0.502	0.49	0.902

IRFs evaluation

The model response for the far-side configuration (Fig. 18) [28] was compared to the PMHS response in terms of force vs. time (contact force between the console and the HBM) (Fig. 19 and Fig. 20) and injury probability (Fig. 21). The liver, spleen and small intestine injury risks were predicted in the simulation using the previous IRFs based on the MPS95 and a Weibull distribution for the liver, spleen, the 95th percentile of the maximal pressure and a Log-Normal distribution for the small intestine. According to Fig. 21, the injury probabilities given by the IRF derived from group 2 matched very well the ones computed from the PMHS experiments. With the IRFs derived from group 1, the injury probabilities deviated from those given by the experiments, but were not that far: 30% vs. 17% for the liver (overestimation), 10% vs. 17% for the spleen (underestimation), and 5% vs. 0% for the small intestine.

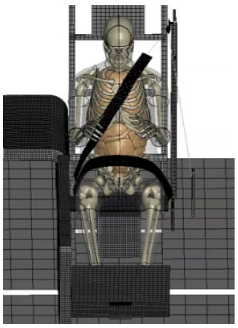

Fig. 18. Far-side configuration.

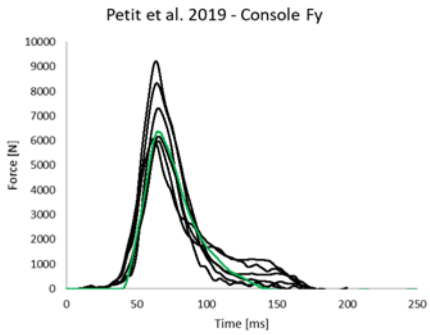

Fig. 19. HBM and PMHS Y-force against the console (HBM response is in green).

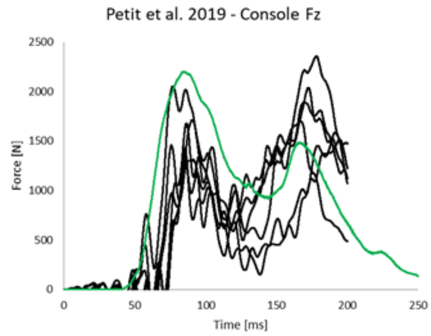

Fig. 20. HBM and PMHS Z-force against the console (HBM response is in green).

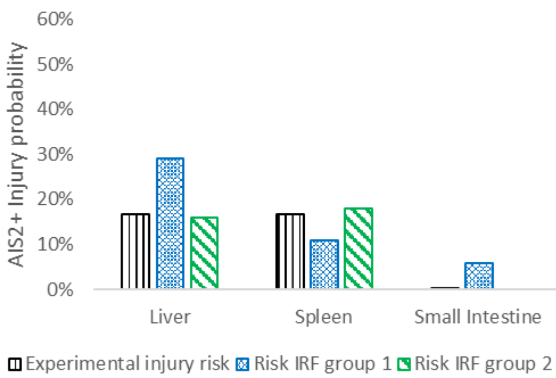

Fig. 21. Experimental probability of injury vs. model prediction.

IV. DISCUSSION

In this study, simulation-based AIS2+ IRFs were developed for the liver, spleen, and the SI of the 50th percentile male THUMS v7 model. A review of the literature collected 177 relevant experimental tests on 145 PMHS, which were replicated with the HBM. Among these tests, 44 resulted in liver injuries, 25 in spleen injuries, and 14 in SI injuries. Different metrics were taken from the HBM abdominal elements and paired with the PMHS injury outcomes. Their relevance for injury prediction was assessed using the AROC scores.

Following the methodology of Beillas *et al.* [7], the IRFs were built using two different samples: a large one (group 1), taking all the metric value-injury outcome paired data points; and a smaller one (group 2), excluding the tests for which the organ involvement was not sure. Although the IRFs based on group 1 yielded satisfactory QI ratings at 5%, 25%, and 50% of risk, better quality rating was achieved with the IRFs based on group 2 (Table IX). Beillas *et al*. [7] also found better rating when using the small sample (called C3 group in their paper). Consequently, the authors of the present paper recommend using the liver and spleen IRFs built on the small sample (group 2), keeping in mind potential limitations. Among these, almost all the frontal loading cases were excluded from group 2. However, given that the metrics are at the tissue level, we consider that these IRFs can be used independently of the loading directions.

TABLE IX
QUALITY INDEX OF THE IRFS FOR THE DIFFERENT GROUPS AND ORGANS

		Group 1			**Group 2**		
Organ	Predictor	QI at 5%	QI at 25%	QI at 50%	QI at 5%	QI at 25%	QI at 50%
Liver	MPS95	Fair	Good	Good	Good	Good	Good
Spleen	MPS95	Marginal	Good	Fair	Fair	Good	Good
SI	Press95	Good	Good	Fair	NA	NA	NA

Only one additional configuration was used to check the ability of the model to predict abdominal injury using the newly developed IRFs. The prediction of the model is well in accordance with the PMHS injury outcome for the liver, spleen and small intestine when using the IRFs from group 2. The IRFs from group 1 are less in accordance with the test outcomes but are relatively close. Compared to the tests, the risk of injury for the liver, spleen, and SI given by THUMS are overestimated, underestimated, and overestimated, respectively. This first result is encouraging, but additional configurations are required with more severe conditions and different loading directions to confirm the correct prediction. Only one configuration is not enough to constitute an assessment of the IRFs. For instance, it could be relevant to add some full-body sled experiments resulting in abdominal injury, per Uriot *et al*. and Baudrit *et al.* [29-30]. The use of some accident reconstructions could also be helpful to increase the confidence on the prediction of these IRFs.

Several assumptions and simplifications were made in our study that could affect the results. No exclusion was performed in the dataset based on the biological sex, i.e. male and female subjects were used to build the IRFs, assuming no sex effect on the injury outcome. The proportion of male and female subjects is presented in Table X. It should be noted that for one subject the biological sex information was not found (Maltese *et al*. [24] experiments, test SIC-08). The proportion of female subjects in the dataset is not negligible and it is not known how the biological sex could affect the abdominal injury outcome. Other parameters, such as the abdominal fat content inside organs, within organs, or subcutaneous, or the abdominal general geometry, could also affect the injury outcome but were not considered in this study. Only the global mass from a subject to another was taken into account by scaling the input parameters before simulation but no personalization of the HBM was performed. Further analysis could be done on this specific aspect by morphing the HBM to provide a better match with the subject anthropometry and evaluate the effect the morphology on the abdominal injury outcome. The mass variations within PMHS were taken into account by scaling the boundary conditions (impactor initial velocity or imposed force) of the configurations before simulation. It is believed that this approach contributed to the consistency of the results. Perez *et al.* [31] generated IRFs to predict the risk of pelvis injuries with the GHBMC M50 model. They performed subject-specific simulations by scaling the impactor initial velocity to expose the model to a severity level equivalent to a given PMHS based on the mass. They evaluated the scaling benefits using the GHBMC M95 and M50 models and found a better correlation between the strain of M50 model and the M95 model using a scaled impactor velocity. Beillas *et al*. [7] also investigated the effect of scaling, using either a baseline M50 GHBMC model or a scaled GHBMC model to match the height, mass and size of the PMHS. However, they did not find improvement on the risk prediction using a scaled model. In our study, the relevance of scaling was not actually investigated. This could also be done in future analysis.

The IRFs presented in this study were developed without age adjustment. As many studies based on PMHS data, a limitation is the advanced age of the subjects. In our dataset, the mean age of the PMHS was 66 yrs. ± 15yrs. for group 1 and 63 yrs. ±14 yrs. for group 2. The liver is for example known as affected by ageing with anatomical changes as a decrease of the organ volume [32]. Example of the IRFs with age adjustment are presented in Appendix (Fig. AI to Fig. IX). However, it is recommended to use the IRFs for an age close to the mean age of the PMHS because the confidence interval become wider when the age is too far for the mean age of the subjects. The IRFs for an age of 65 years old are very close to the IRFs without age adjustment.

The initial posture is known as a parameter affecting the HBM response [33]. In this study, the HBM was positioned to match the PMHS posture from visual inspection but no subject-specific positioning was done. It is unclear to what extent it could affect the response at organ level, and the results could be slightly different with a better posture personalized. A sensitivity analysis could be performed as a next step to evaluate robustness of the injury probability predicted by the model with regard to some posture adjustments.

TABLE X
PROPORTION OF MALE AND FEMALE SUBJECTS

	Proportion of Male	**Proportion of Female**
Group 1	64%	35%
Group 2	56%	43%

To decrease the volume of simulations and save some computational time, some of the subject-specific simulations for a given configuration were not started. Instead, a relationship between the metrics value and the test boundary conditions was established by regression on the simulated tests, and the metric value for the non-started simulation was estimated using the regression. This was mainly done for the impactor simulations when the imposed initial velocity was changed without other modifications. A check of this approximation was done using the Hardy *et al.* [13] bar impact test configuration. Four simulations were run with an initial velocity of the impactor of 5.7 m/s, 7.2 m/s, 9 m/s and 10.8 m/s. For each of these simulations, the liver MPS95 was extracted and a linear regression was carried out between the MPS95 values and the initial velocity of the impactor (without using the simulation at 7.2 m/s). Then, the MPS95 value for the impact at 7.2 m/s coming from the simulation was compared to the liver MPS95 value using the relationship (Table XI). This configuration was chosen to evaluate the method because in that case the differences on the impactor initial velocity are quite large. Still the MPS95 value from the simulation and that predicted using the regression are really close, with a difference of 3.5%. This error was considered acceptable to save computational time and the approach was used for other similar loading cases (regression results are presented in Table AVII for the different configurations).

TABLE XI
MEASURED PARAMETERS

Impactor initial velocity [m/s]	**Liver MPS95 from simulation**	**Liver MPS95 interpolated from regression**
5.8	0.338	-
7.2	0.393	0.407
9	0.495	-
10.8	0.586	-

In our selected experimental dataset, only four subjects sustained kidney injuries and two subjects sustained stomach injuries. Due to the limited amount of data for these organs, it was not possible to develop IRFs. Similarly, only seven subjects sustained injuries on the large intestine and it was not possible to develop an IRF. Further research and experiments focusing more on these organs will be required to gain a better understanding of their injury tolerance and to implement injury criteria in HBM. For the SI, all the injuries but one came from abdominal loading with a seat belt.

The Confidence Interval for the SI is fair at 50% risk, but becomes larger after this risk level. More understanding of the SI injury mechanisms/tolerance is required. Similar tendency is observed with the spleen IRF after 60% probability of injury. The comparison between the parametric and the non-parametric IRFs presents the same conclusion and highlights the poor quality of the fit after 50% risk for the spleen and the SI. This could be explained by the small amount of injurious data compared to the number of non-injurious data, especially for the spleen and SI. Hence, after 50% of SI or spleen injury probability with the given IRFs, the results should be interpreted with caution.

More monitoring is required to evaluate the performance of the prediction using group 2 or group 1. Again, real accident reconstructions with and without abdominal organs injury would be very helpful in this process.

As a perspective of this study, similar work could be performed to develop abdominal organ IRFs for the THUMS v7 05th percentile female model and other models from the THUMS family.

V. CONCLUSION

New simulation-based IRFs were developed for the liver, spleen and the small intestine with M50 THUMS v7 model. The liver and spleen IRFs are based on the MPS95 extracted on the solid elements of the organs with a Weibull distribution. The small intestine IRF is based on the 95th percentile of the pressure extracted on the shell element of the organ with a Log-Normal distribution. The QI of Liver, Spleen and SI at 25% of risk are good. First results are encouraging, but more data are required to fully validate the IRFs. To that end, further simulations based on real car accidents could help in the assessment of injury prediction. Furthermore, this study highlights the need to perform new experiments dedicated to the abdominal injuries study, especially for the kidneys and the intestines.

VI. ACKNOWLEDGEMENTS

We would like to thank Sabine Compigne for her contribution in setting up this study. We also thank the members of Toyota Motor Company and Toyota Motor Europe for their support and contributions throughout this project.

VII. REFERENCES

[1] Weaver, A. A., Talton, J. W., *et al*. (2015) Estimated Injury Risk for Specific Injuries and Body Regions in Frontal Motor Vehicle Crashes. *Traffic Injury Prevention*, **16**: pp. 108–116.

[2] Klinich, K., Flannagan, C. A. C, Nicholson, K., Schneider, L. W., Rupp, J. D. (2008) Abdominal Injury in Motor-Vehicle Crashes. University of Michigan Transportation Research Institute.

[3] Lamielle, S., *et al*. (2006) Abdominal injury patterns in real frontal crashes: influence of crash conditions, occupant seat and restraint systems. *Annual Proceedings of the Association for the Advancement of Automotive Medicine*, **50**: pp. 103–118.

[4] Albert, D. L., Guettler, A. J., Kemper, A. R., Hardy, W. N. (2024) Evaluation of Abdominal Injury Risk Prediction from Seatbelt Loading. *Proceedings of the IRCOBI Conference*, 2024, Stockholm, Sweden.

[5] Ramachandra, R., Kang, Y.-S., *et al*. (2016) Biomechanical Responses of PMHS Subjected to Abdominal Seatbelt Loading. *Stapp Car Crash Journal*, **60**: pp. 59–87

[6] Wang, Z. J., Hu, G. (2024) Investigation of Pressure-based Abdomen Injury Risk Function with Postmortem Human Subject and Porcine Data for THOR-AV 50M Dummy. *Proceedings of the IRCOBI Conference*, 2024, Stockholm, Sweden.

[7] Beillas, B., Berthet, F. (2018) Development of Simulation-Based Liver and Spleen Injury Risk Curves for the GHBMC Detailed Models. *Proceedings of the IRCOBI Conference*, 2018, Athens, Greece.

[8] Matsuda, T., Kobayashi, N., Fujita, N., Kitagawa, Y. (2023) Development of a human body model (THUMS version 7) to simulate kinematics and injuries of reclined occupant in frontal collision. Paper No. 23-0030. *Proceedings of the 27th International Technical Conference on the Enhanced Safety of Vehicles*, 2023, Yokohama, Japan.

[9] Sahoo, D., Jani, D., Marini, G. (2024) Validation THUMSv4.1 head model in Visual Performance Solution and development of model-specific head injury criteria: skull fracture, mild Diffuse Axonal injury and subdural haematoma. *Proceedings of the IRCOBI Conference*, 2024, Stockholm, Sweden.

[10] Forman, J., *et al*. (2012) Predicting Rib Fracture Risk with Whole-Body Finite Element Models: Development and Preliminary Evaluation of a Probabilistic Analytical Framework. *Proceedings of the 56th AAAM Annual Conference on Annals of Advances in Automotive Medicine*, 2012, **56**: pp. 102–124.

[11] Forman, J., Kulkarni, S., *et al*. (2022) A Method for Thoracic Injury Risk Function Development for Human Body Models. *Proceedings of the IRCOBI Conference*, 2022, Porto, Portugal.

[12] AAAM (2015) The Abbreviated Injury Scale 2015 Revision. *Version 6 October 2016. Association for the Advancement of Automotive Medicine.* 35 E Wacker Drive Ste. 850 – Chicago, Illinois 60601 USA. Web address: http://www.aaam.org/

[13] Hardy, W. N., Schneider, L. W., Rouhana, S. W. (2001) Abdominal impact response to rigid-bar, seatbelt, and airbag loading. *Stapp Car Crash Journal*, **45**: pp. 1–31.

[14] Nusholtz, G. S., Kaiker, P. S., Lehman, J. (1988) Steering system abdominal impact trauma. MVMA Project No. 7131 Final UMRTI Report.

[15] Cavanaugh, J. M., Nyquist, G. W., Goldberg, S. J., King, A. I. (1986) Lower abdominal tolerance and response. *Proceedings of the 30th Stapp Car Crash Conference*, San Diego, USA, pp. 41–63.

[16] Trosseille, X., Le-Coz, J.-Y., Potier, P., Lassau, J.-P. (2002) Abdominal response to high-speed seatbelt loading. *Stapp Car Crash Journal*, **46**: pp. 71–79.

[17] Lamielle, S., Vezin, P., *et al*. (2008) 3D deformation and dynamics of the human cadaver abdomen under seatbelt loading. *Stapp Car Crash Journal*, **52**: pp. 267–294.

[18] Foster, C. D., Hardy, W. N., Yang, K. H., King, A. I., Hashimoto, S. (2006) High-speed seatbelt pretensioner loading of the abdomen. *Stapp Car Crash Journal*, **50**: pp. 27–51.

[19] Howes, M. K., Hardy, W. N., Agnew, A. M., Hallman, J. J. (2015) Evaluation of the Kinematic Responses and Potential Injury Mechanisms of the Jejunum during Seatbelt Loading. *Stapp Car Crash Journal*, **59**: pp. 225–267.

[20] Viano, D. C., Lau, I. V., Asbury, C., King, A. I., Begeman, P. C. (1989) Biomechanics of the human chest, abdomen, and pelvis in lateral impact. *Proceeding of the 33rd Annual Meeting of the Association for the Advancement of Automotive Medicine*, pp. 367–382.

[21] Kremer, M. A., Gustafson, H. M., Bolte, J. H., Stammen, J., Donnelly, B. (2011) Pressure-based abdominal injury criteria using isolated liver and full-body post-mortem human subject impact test. *Stapp Car Crash Journal*, **55**: pp. 3117–3150.

[22] Walfisch, G., Fayon, A., *et al.* (1980) Designing of a dummy's abdomen for detecting injuries in side impact collisions. *Proceedings of the IRCOBI Conference*, 1980, Birmingham, England.

[23] Cavanaugh, J. M., Walilko, T., Chung, J., King, A. I. (1996) Abdominal injury and response in side impact. *Proceedings of the Stapp Car Crash Conference*, pp. 1–16.

[24] Maltese, M., R., Eppinger, R., H., *et al.* (2002) Response Corridors of Human Surrogates in Lateral Impacts. *Stapp Car Crash Journal*, **46**: pp. 321–351.

[25] Petitjean, A., Trosseille, X., Praxl, N., Hynd, D., Irwin, A. (2009) Injury risk curves for the WorldSID 50th male dummy. *Stapp Car Crash Journal*, **53**: pp. 443–476.

[26] Eppinger, R. H. (1976) Prediction of thoracic injury using measurable experimental parameters. *Proceedings of the 6th International Technical Conference on Experimental Safety Vehicles*, pp. 770–779. NHTSA, Washington, D.C.

[27] Petitjean, A., Trosseille, X., Yoganandan, N., Pintar, F. A. (2015) Normalization and Scaling for Human Response Corridors and Development of Injury Risk Curves. In: Yoganandan, N., Nahum, A. M., Melvin, J. W, (editors), *Accidental Injury: Biomechanics and Prevention*, Third ed. Springer: New York NY, pp. 769–792.

[28] Petit, P., *et al*. (2019) Far Side Impact Injury Threshold Recommendations Based on 6 Paired WorldSID / Post Mortem Human Subjects Tests. *Stapp Car Crash Journal*, **63**: pp. 127–146.

[29] Uriot, *et al*. (2015) Reference PMHS Sled Tests to Assess Submarining. *Stapp Car Crash Journal*, **59**: pp. 203–223.

[30] Baudrit, P., Uriot, J., Richard, O., Debray, M. (2022) Investigation of Potential Injury Patterns and Occupant Kinematics in Frontal Impact with PMHS in Reclined Postures. *Stapp Car Crash Journal*, **56**: pp. 1–30.

[31] Peres, J., Auer, S., Praxl, N. (2016) Development and comparison of different injury risk functions predicting pelvic fractures in side impact for a Human Body Model. *Proceedings of the IRCOBI Conference*, 2016, Malaga, Spain.

[32] Parenteau, C. S, Ehrlich, P., Ma, L., Su, G., L., Holcombe, S., Wang, S. C. (2013) The Quantification of Liver Anatomical Changes and Assessment of Occupant Liver Injury Patterns. *Stapp Car Crash Journal*, **57**: pp. 267–283.

[33] Poulard, D., Subit, D., Nie, B., Donlon, J.-H., Kent, R. W. (2015) The Contribution of Pre-impact Posture on Restrained Occupant Finite Element Model Response in Frontal Impact. *Traffic Injury Prevention*, **16**(Suppl 2): pp. 87–95.

VIII. APPENDIX

Impactor and « impactor liked » experiments

Viano *et al*. [20] performed a series of impacts on PMHS with a 23.4 kg cylindrical impactor in free flight condition. Several impact configurations were conducted with different impactor speeds [3.62 m/s;10.2 m/s], different impact angles with respect to the sagittal plane of the PMHS (oblique or lateral), and different impacted body region (thorax or abdomen). Some PMHS were impacted several times.

Cavanaugh *et al*. [15] performed a series of experiments in which the PMHS were seated on a horizontal platform and loaded by an impactor (free flight condition), which head was a rigid bar orientated so that the long axis of the bar was parallel to the width of the body. The dimension of the bar was 381 mm long, and 25 mm in diameter. Two impacting masses were used, either ~31.2 kg or 63.6 kg, and the impact velocity ranged from 4.87 m/s to 13.01 m/s.

Kremer *et al.* [21] conducted PMHS impacts with an aluminum striker (rectangular plate of 15 cm x 30 cm) impacting the abdomen of the subjects. The total impactor mass was 23.1 kg. At time to contact, the guided impactor was in a free flight condition. The tests onto the abdomen were pure lateral or oblique (30 degrees forward) with an initial velocity of the impactor close to 7 m/s.

Hardy *et al.* [13] conducted typical free-back test configurations in which the PMHS abdomen was impacted by a 2.5 cm diameter rigid bar. The impacting mass was 48 kg and corresponds to the median of the masses used in the Cavanaugh [15] experiments. Three impact velocity ranges were used: 4.3 m/s, 6.0m/s, and 9.0 m/s.

Nusholtz *et al*. [14] conducted impact test in free flight condition with a 18 kg pendulum equipped at its head with a rigid lower rim of a steering wheel. The impact velocity ranged from 1.3 m/s to 10.8 m/s and three contact regions against the abdomen were used. Each PMHS was impacted several times.

Hardy *et al*. [13] conducted experiments to mimic a deploying airbag impact against the abdomen by propelling a lightweight 1 kg impactor. The striking surface was the sidewall of a 7.6 cm diameter tube that is 20 cm long. The ends of the cylinder were fitted with rounded caps to help eliminate edge loading of the abdomen as penetration increases. The cylinder was attached to a 5 cm diameter shaft that was 30 cm long. The impactor velocity ranged from 10.7 m/s to 13.6 m/s and its course was 76 mm.

Walfish *et al.* [22] performed drop tests on PMHS. The test set-up consisted of a horizontal, flat and rigid surface equipped with an armrest. The PMHS was dropped laterally with an impact against the armrest at the level of the 9th right rib (the right arms of the PMHS were maintained such they did not interact with the armrest). The drop height was 1 m or 2 m. The protrusion of the armrest varied from 31 mm to 55 mm.

Abdominal loading with belt

Ramachandra *et al*. [5] conducted abdominal loading on PMHS with lap belt. The seat belt was positioned on the abdomen, above the iliac crests at the level of the umbilicus, with a 10–20 N preload belt tension. The two strands of the seat belt were fixed onto a rigid ram that was suddenly pulled back at approximately 4.2 ± 0.5 m/s. The pelvis and legs of the PMHS rested onto a flat, horizontal and frictionless surface.

Hardy *et al.* [13] conducted abdominal loading on PMHS with lap belt. The PMHS were seated upright with the legs outstretched, supported by a Teflon skid, with the hands positioned above the head. The belt was placed at the mid-abdominal region, approximately at the level of the umbilicus.

Trosseille *et al.* [16] conducted abdominal loading of PMHS by pulling a lap belt. The subjects were seated on a static rigid seat and back support. The belt strands were routed backward by prototype pretensioners. Two test configurations were used. Configuration 1 was a single-sided pretension: only one strand of the belt was loaded. Configuration 2 was a dual-sided pretension: both strands of the belt were loaded, each with an identical pretensioner triggered simultaneously.

Lamielle *et al*. [17] conducted abdominal loading of PMHS by pulling a lap belt. The subjects were seated on a static rigid seat and back support. The belt strands were symmetrically routed backward by a loading device through pulleys. Two types of loading device were used.

Foster *et al*. [18] conducted abdominal loading of PMHS by pulling a lap belt. The apparatus consisted of a rigid back support, a seat-belt pretensioner system, and a belt-guide roller mechanism. The belt was routed straight back from the sides of the PMHS. Symmetric loading (right- and left-side retraction) was implemented to reduce torsion and shear effects. Three pretensioner systems were used, denoted A, B, and C. The systems consisted of either a single (B and C) or a dual (A) pretensioner.

Howes *et al.* [19] conducted a series of PMHS loading with a 3-point seat belt. The tests were conducted in a fixed-back configuration where the C5 and L3 vertebrae of the PMHS were attached to a rigid and motionless frame facing to the spine. The separated lap and shoulder belts were pulled rearward through rollers, with the lap belt routed superior to the pelvis. Belt motion was driven by a pneumatic linear impactor for a target peak belt speed of 3 m/s. Four tests were conducted with the PMHS in an inverted position, and two tests were conducted with the PMHS upright.

Lateral sled

Maltese *et al*. [24] reported a series of lateral impacts on PMHS against a wall fixed on a sled. The seat was covered with a low friction surface and the seatback was composed on three cylindric bars, respectively positioned at the pelvis, thoracic and head levels. The velocity of the impact wall was either 6.7 m/s or 8.9 (± 0.3) m/s. The sled carrying the impacting wall continued to move along its track at near-constant velocity during occupant-to-load wall interaction. The sled was then gradually slowed by a braking system. The impacting wall was composed of four plates that could be either rigid (R), or covered (P) with 10 cm of LC200 padding (compressive stiffness = 103 kPa, equivalent padding presented in Petit *et al.* 2019 [28]). A 11 cm offset toward the subject is also be applied either to the thoracic plate (OT), or the abdomen plate (OA), or the pelvic plate (OP). The configuration with all the plates in the same plane (F) was also used.

Many tests performed with this test buck can be found in NHTSA biomechanics database. Maltese *et al*. [24] described the wall geometries and selected tests to propose biofidelity corridors. Petitjean *et al.* (2009) [25] also screened the NHTSA database and selected tests to build injury risk curves for the WorldSID dummy. This is the selection of Petitjean *et al.* that was used for the present study (N=39, see TABLE AIV), including those that were not replicated with the dummy. Tests from NHTSA database not included in the sample were rejected on the basis of the following criteria:

- inconsistency in the change of momentum between tests.
- transmissibility irregularities between the thorax and the pelvis in the tests.
- position of the PMHS not quite parallel to the wall at the time of impact (excessive leaning).

Cavanaugh *et al*. [23] performed a series of lateral impact PMHS tests. The test set-up consisted of a wall fixed on a sled. At time zero, the sled and the PMHS were accelerated in order to reach 6.7 m/s or 8.9 m/s. The sled was suddenly decelerated upon impacting a hydraulic damper. At the same time, the PMHS slides across a frictionless seat into a wall equipped with load cells. Flat rigid wall and armrest tests were performed. The armrest fixture consisted of paper honeycombs with different mechanical characteristics (soft and stiff), depending on the tests.

TABLE AI

EXPERIMENTAL CONFIGURATIONS AND BOUNDARY CONDITION FOR SIMULATIONS (IMPACTOR TESTS)

Reference	Configuration	Boundary Condition	Model
Cavanaugh *et al.* [15]	31 kg bar impact at the level of L3	Free back condition. Imposed initial velocity on the impactor	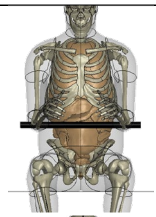
Cavanaugh *et al*. [15]	48 kg bar impact at the level of T11	Free back condition. Imposed initial velocity on the impactor	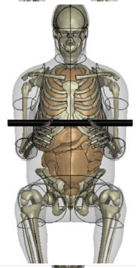
Hardy *et al.* [13]	48 kg bar impact at the level of L3	Free back condition. Imposed initial velocity on the impactor	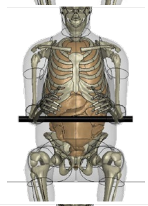
Cavanaugh *et al*. [15]	63 kg bar impact at the level of L3	Free back condition. Imposed initial velocity on the impactor	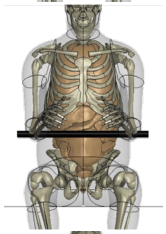
Cavanaugh *et al*. [15]	63 kg bar impact at the level of L1	Free back condition. Imposed initial velocity on the impactor	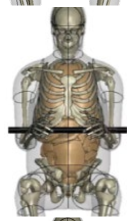
Hardy *et al.* [13]	Airbag-like impactor (1 kg) Impact location at mid-abdomen	Fixed back condition. Imposed initial velocity on the impactor. Impactor course: 76 mm	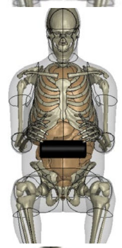
Viano *et al*. [20]	23 kg cylindrical impactor. Impact location: Left lateral at Xiphoid level	Imposed initial velocity on the impactor	
Viano *et al*. [20]	23 kg cylindrical impactor. Impact location: Left oblique (30 degrees) at Xiphoid level	Imposed initial velocity on the impactor	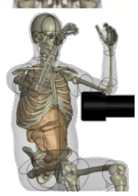

TABLE AI

EXPERIMENTAL CONFIGURATIONS AND BOUNDARY CONDITION FOR SIMULATIONS (IMPACTOR TESTS)

Viano *et al*. [20]	23 kg cylindrical impactor impact location: Left oblique (30 degrees) at abdomen level	Imposed initial velocity on the impactor	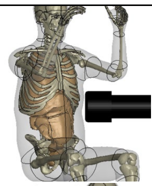
Viano *et al*. [20]	23 kg cylindrical impactor. Impact location: Right Oblique (30 degrees) at Xiphoid level	Imposed initial velocity on the impactor	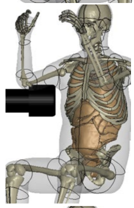
Viano *et al*. [20]	23 kg cylindrical impactor. Impact location: Right Oblique (30 degrees) at abdomen level	Imposed initial velocity on the impactor	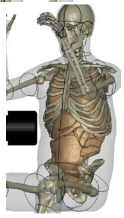
Kremer *et al.* [21]	23.1 kg Rectangular impactor. Impact location: Right lateral at abdomen (centre of impactor 5.08 cm below the xyphoid process)	Imposed initial velocity on the impactor	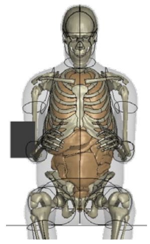
Kremer *et al*. [21]	23.1 kg Rectangular impactor. Impact location: Right Oblique (30 degrees) at abdomen (centre of impactor 5.08 cm below the xyphoid process)	Imposed initial velocity on the impactor	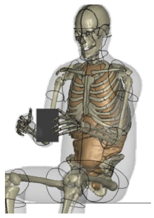
Walfish *et al*. [22]	Drop test of PMHS on rigid armrest. The armrest faced to the 9th rib.	Imposed force vs. time curve on the rigid armrest (low mass) to reproduce the loading	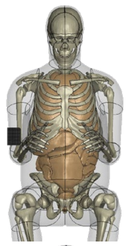
Nusholtz *et al*. [14]	18 kg steering-wheel impact at the level of the abdomen	Imposed velocity on the impactor	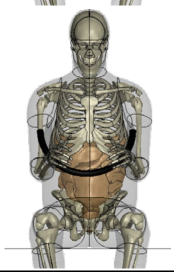

TABLE AII
EXPERIMENTAL CONFIGURATIONS AND BOUNDARY CONDITION FOR SIMULATIONS (ABDOMINAL LOADING WITH BELT)

Reference	Configuration	Boundary Condition	Model
Foster *et al*. [18]	Abdominal loading at the mid-umbilical level with a lap belt	Force vs. time imposed on the belt extremities. Fixed back condition	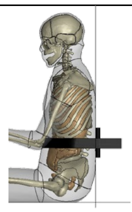
Lamielle *et al*. [17]	Abdominal loading at the mid-umbilical level with a lap belt	Force vs. time imposed on the belt extremities. Fixed back condition	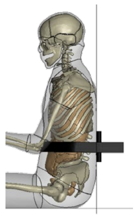
Hardy *et al.* [13]	Abdominal loading at the mid-umbilical level with a lap belt	Force vs. time imposed on the belt extremities	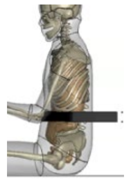
Ramachandra *et al.* [5]	Abdominal loading at the mid-umbilical level with a lap belt	Force vs. time imposed on the belt extremities	
Trosseille *et al*. [16]	Abdominal loading at the mid-umbilical level with a lap belt	Force vs. time imposed on the belt extremities. Fixed back condition	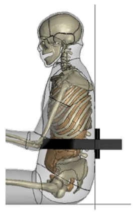
Howes *et al*. [19]	Abdominal and thoracic loading via a three-point belt. C5 and L3 attached to a rigid frame. Two configurations (upright and inverted)	Force vs. time imposed on the belt extremities. Only the upright configuration was used and kept for the inverted configuration. Fixed back condition	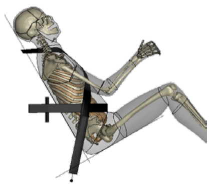

TABLE AIII

EXPERIMENTAL CONFIGURATIONS AND BOUNDARY CONDITION FOR SIMULATIONS (LATERAL SLED)

Reference	Configuration	Boundary Condition	Model
Cavanaugh *et al.* [23]	Lateral sled. Impact on the left side against a rigid wall at 6.7 m/s or 9 m/s	Initial velocity on the HBM (6.7 m/s or 9 m/s)	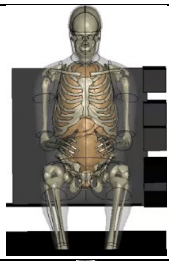
Cavanaugh *et al.* [23]	Lateral sled. Impact on the left side against a padded wall at (152 mm or 102 mm “soft” padding 8.7 m/s	Initial velocity on the HBM (8.7 m/s)	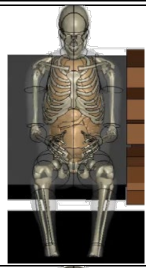
Cavanaugh *et al.* [23]	Lateral sled. Impact on the left side against a padded wall at (102 mm “stiff” padding 8.9 m/s	Initial velocity on the HBM (8.9 m/s)	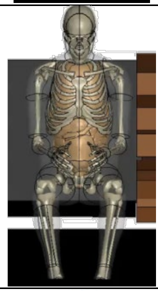
Maltese *et al.* [24]	Lateral sled. Impact on the left side against a rigid wall at 6.7 m/s or 8.9 m/s	Initial velocity on the HBM (6.7 m/s or 8.9 m/s)	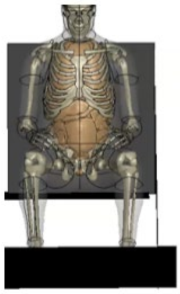
Maltese *et al*. [24]	Lateral sled. Impact on the left side against a padded wall at 6.7 m/s or 8.9 m/s	Initial velocity on the HBM (6.7 m/s or 8.9 m/s)	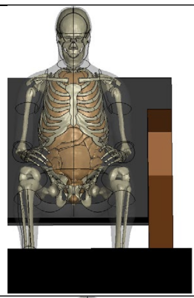
Maltese *et al*. [24]	Lateral sled. Impact on the left side against a rigid wall with an offset of the thoracic, abdominal or pelvis plate	Initial velocity on the HBM (6.7 m/s or 8.9 m/s)	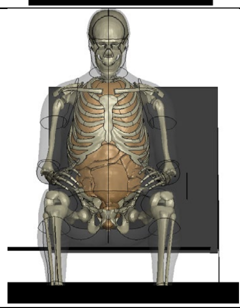

TABLE AIV
PMHS OVERVIEW AND APPLIED DATA CENSORING
Note on censoring status: 0: Right censored data, 2: Left censored data, 3: interval censored data

Study	Configuration	PMHS n°	Number of tests	Age [yrs]	Sex	Weight [kg]	Liver censoring	Spleen censoring	SI censoring
Hardy *et al*. [13]	Bar impact 48 kg T11	28800	1	64	F	61	2	0	0
Hardy *et al*. [13]	Bar impact 48 kg T11	29115	1	74	M	75	2	2	0
Hardy *et al*. [13]	Bar impact 48 kg T11	29084	1	64	M	65	2	0	0
Cavanaugh *et al.* [15]	Bar impact 31 kg L3	525	1	57	M	45	0	0	0
Cavanaugh *et al.* [15]	Bar impact 31 kg L3	473	1	43	F	53	0	0	0
Cavanaugh *et al.* [15]	Bar impact 31 kg L3	590	1	51	F	68	0	0	0
Cavanaugh *et al.* [15]	Bar impact 31 kg L3	684	1	50	M	88	0	0	0
Cavanaugh *et al.* [15]	Bar impact 31 kg L3	786	1	60	M	79	0	0	0
Cavanaugh *et al.* [15]	Bar impact 31 kg L3	751	1	64	M	90	0	0	0
Cavanaugh *et al.* [15]	Bar impact 31 kg L3	977	1	57	F	75	0	0	0
Cavanaugh *et al.* [15]	Bar impact 31 kg L3	731	1	58	M	92	0	0	0
Cavanaugh *et al.* [15]	Bar impact 31 kg L3	739	1	43	M	61	0	0	0
Cavanaugh *et al.* [15]	Bar impact 31 kg L3	721	1	66	M	70	0	0	0
Cavanaugh *et al.* [15]	Bar impact 31 kg L3	712	1	51	F	55	2	2	0
Hardy *et al.* [13]	Airbag-like impact	29490	4	68	F	57	3	0	0
Hardy *et al.* [13]	Airbag-like impact	29566	1	86	M	79	0	0	0
Hardy *et al.* [13]	Airbag-like impact	29491	1	72	M	81	2	0	0
Viano *et al*. [20]	Left Lateral impact Xiphoid	863	1	49	M	107	0	0	0
Viano *et al*. [20]	Left Lateral impact Xiphoid	RNY1	1	76	F	44	0	0	0
Viano *et al*. [20]	Multiple impacts	986	4	29	M	70	3	0	0
Viano *et al*. [20]	Multiple impacts	063	2	64	M	48	3	0	0
Viano *et al*. [20]	Multiple impacts	935	1	63	M	69	0	0	0
Viano *et al*. [20]	Multiple impacts	UOM1	2	37	M	67	0	3	0
Viano *et al*. [20]	Multiple impacts	008	2	52	F	53	0	0	0
Viano *et al*. [20]	Multiple impacts	UOM2	4	64	M	75	0	0	0
Viano *et al*. [20]	Multiple impacts	956	2	40	F	76	0	0	0
Viano *et al*. [20]	Multiple impacts	947	2	38	M	56	0	0	0
Viano *et al*. [20]	Multiple impacts	954	2	66	M	56	0	0	0
Viano *et al*. [20]	Multiple impacts	RNY2	2	64	M	61	0	0	0
Viano *et al*. [20]	Multiple impacts	047	3	62	M	83	0	0	0
Viano *et al*. [20]	Multiple impacts	993	2	49	M	70	0	0	0
Foster *et al*. [18]	Lap-belt loading config. A	31658	1	24	M	96	2	2	0
Foster *et al*. [18]	Lap-belt loading config. A	31996	1	58	M	111	0	0	0
Foster *et al*. [18]	Lap-belt loading config. A	750	1	80	M	57	2	0	0
Foster *et al*. [18]	Lap-belt loading config. A	32016	1	83	M	81	2	0	0
Foster *et al*. [18]	Lap-belt loading config. B	31719	1	85	M	80	0	0	0
Foster *et al*. [18]	Lap-belt loading config. B	623	1	45	M	74	0	0	0
Foster *et al*. [18]	Lap-belt loading config. B	694	1	59	M	62	0	0	0
Foster *et al*. [18]	Lap-belt loading config. C	31860	1	86	F	37	0	0	0
Lamielle *et al.* [17]	Lap-belt loading MHA	MS586	1	74	M	77	0	2	0
Lamielle *et al.* [17]	Lap-belt loading MHA	MS587	1	82	M	78	2	0	2
Lamielle *et al.* [17]	Lap-belt loading MHA	MS588	1	88	M	69	0	0	2
Lamielle *et al.* [17]	Lap-belt loading MHA	MS589	1	88	M	60	0	0	2
Lamielle *et al.* [17]	Lap-belt loading PRT	MS580	1	72	M	54	0	0	2
Lamielle *et al.* [17]	Lap-belt loading PRT	MS581	1	85	M	56	0	0	2
Lamielle *et al.* [17]	Lap-belt loading PRT	MS582	1	88	M	72	2	2	2
Lamielle *et al.* [17]	Lap-belt loading PRT	MS583	1	82	M	77	0	2	2
Hardy *et al.* [13]	Lap-belt loading	29311	1	77	F	53	0	0	0
Hardy *et al.* [13]	Lap-belt loading	29116	1	78	M	52	0	0	0
Hardy *et al.* [13]	Lap-belt loading	29131	1	88	M	72	0	0	0
Ramachandra *et al.* [5]	Lap-belt loading	01	1	59	M	86	0	2	0
Ramachandra *et al.* [5]	Lap-belt loading	02	1	66	F	64	0	0	0
Ramachandra *et al.* [5]	Lap-belt loading	03	1	66	M	70	0	0	0
Ramachandra *et al.* [5]	Lap-belt loading	06	1	25	M	74	0	0	0
Ramachandra *et al.* [5]	Lap-belt loading	07	2	48	M	67	0	0	3
Ramachandra *et al.* [5]	Lap-belt loading	04	2	80	M	86	0	0	0
Ramachandra *et al.* [5]	Lap-belt loading	05	2	75	F	50	0	0	0

TABLE AIV

PMHS OVERVIEW AND APPLIED DATA CENSORING

Note on censoring status: 0: Right censored data, 2: Left censored data, 3: interval censored data

Trosseille *et al.* [16]	Lap-belt loading	MS515	1	66	F	68	0	0	0
Trosseille *et al.* [16]	Lap-belt loading	MS517	1	64	F	45	0	0	0
Trosseille *et al.* [16]	Lap-belt loading	MS520	1	86	F	50	0	0	0
Trosseille *et al.* [16]	Lap-belt loading	MS503	1	76	M	78	0	0	0
Trosseille *et al.* [16]	Lap-belt loading	MS505	1	81	M	70	0	0	2
Trosseille *et al.* [16]	Lap-belt loading	MS507	1	85	M	51	2	2	0
Kremer *et al*. [21]	Right lateral impact	FBL03-L	1	88	M	73	2	0	0
Kremer *et al*. [21]	Right lateral impact	FBL11-L	1	65	F	54	0	0	0
Kremer *et al*. [21]	Right lateral impact	FBL01-L	1	68	M	67	2	0	0
Kremer *et al*. [21]	Right lateral impact	FBL02-L	1	80	F	59	0	0	0
Kremer *et al*. [21]	Right lateral impact	FBL04-L	1	91	M	64	0	0	0
Kremer *et al*. [21]	Right lateral impact	FBL05-O	1	53	F	54	2	0	0
Kremer *et al*. [21]	Right lateral impact	FBL06-O	1	79	M	82	2	0	0
Kremer *et al*. [21]	Right lateral impact	FBL07-O	1	82	M	57	2	0	0
Kremer *et al*. [21]	Right lateral impact	FBL08-O	1	77	F	69	2	0	0
Kremer *et al*. [21]	Right lateral impact	FBL09-O	1	78	F	58	2	0	0
Walfish *et al*. [22]	Drop test	205	1	62	F	32	0	0	0
Walfish *et al*. [22]	Drop test	206	1	66	M	82	2	0	0
Walfish *et al*. [22]	Drop test	215	1	52	M	53	2	0	0
Walfish *et al*. [22]	Drop test	217	1	55	M	58	2	0	0
Hardy *et al.* [13]	Bar impact 48 kg L3	28838	1	85	M	91	2	2	0
Hardy *et al.* [13]	Bar impact 48 kg L3	28764	1	93	F	58	2	0	0
Hardy *et al.* [13]	Bar impact 48 kg L3	28942	1	85	F	51	2	2	0
Hardy *et al.* [13]	Bar impact 48 kg L3	28682	1	87	M	73	2	0	0
Hardy *et al.* [13]	Bar impact 48 kg L3	28889	1	71	M	64	2	0	0
Hardy *et al.* [13]	Bar impact 48 kg L3	28879	1	74	M	77	0	0	0
Howes *et al*. [19]	3-pt belt loading	SM101	1	73	M	53	0	0	2
Howes *et al*. [19]	3-pt belt loading	SM102	1	78	M	50	2	0	0
Howes *et al*. [19]	3-pt belt loading	SM103	1	87	M	33	0	0	2
Howes *et al*. [19]	3-pt belt loading	SM104	1	76	M	74	0	0	2
Howes *et al*. [19]	3-pt belt loading	SM106	1	87	M	58	2	0	2
Howes *et al*. [19]	3-pt belt loading	SM108	1	85	M	66	2	0	2
Cavanaugh *et al*. [23]	Lat. sled 102 mm stiff pad	NA	1	61	F	54	0	0	0
Cavanaugh *et al*. [23]	Lat. sled 102 mm stiff pad	NA	1	68	F	54	0	0	0
Cavanaugh *et al*. [23]	Lat. sled 102 mm stiff pad	NA	1	72	M	55	0	2	0
Cavanaugh *et al*. [23]	Lat. sled 102 mm stiff pad	NA	1	58	F	56	0	2	0
Cavanaugh *et al*. [23]	Lat. sled 102 mm soft pad	NA	1	62	M	66	0	0	0
Cavanaugh *et al*. [23]	Lat. sled 102 mm soft pad	NA	1	43	F	68	0	0	0
Cavanaugh *et al*. [23]	Lat. sled 152 mm soft pad	NA	1	60	M	62	0	0	0
Cavanaugh *et al*. [23]	Lat. sled 152 mm soft pad	NA	1	54	F	55	0	0	0
Cavanaugh *et al*. [23]	Lat. sled 152 mm soft pad	NA	1	65	M	93	0	0	0
Cavanaugh *et al*. [23]	Lateral sled rigid wall	217	1	67	M	44	0	0	0
Cavanaugh *et al*. [23]	Lateral sled rigid wall	206	1	66	M	74	0	0	0
Cavanaugh *et al*. [23]	Lateral sled rigid wall	UM12	1	64	F	73	0	2	0
Cavanaugh *et al*. [23]	Lateral sled rigid wall	215	1	69	M	57	0	2	0
Cavanaugh *et al*. [23]	Lateral sled rigid wall	216	1	60	M	61	0	0	0
Maltese *et al*. [24]	Lateral sled padded High vel.	SC134	1	58	F	62	0	0	0
Maltese *et al*. [24]	Lateral sled padded High vel.	SC107	1	50	M	93	0	0	0
Maltese *et al*. [24]	Lateral sled padded High vel.	W9303	1	59	F	81	2	2	0
Maltese *et al*. [24]	Lateral sled padded High vel.	W9306	1	82	F	74	2	2	0
Maltese *et al*. [24]	Lateral sled padded High vel.	W9312	1	80	F	45	2	0	0
Maltese *et al*. [24]	Lateral sled padded High vel.	SC133	1	73	M	74	2	0	0
Maltese *et al*. [24]	Lateral sled padded High vel.	SC116	1	67	M	76	0	0	0
Maltese *et al*. [24]	Lateral sled padded High vel.	W9314	1	79	M	67	2	2	0
Maltese *et al*. [24]	Lateral sled padded High vel.	LSI32P15	1	68	F	54	0	0	0
Maltese *et al*. [24]	Lateral sled padded High vel.	LSI32P16	1	77	F	48	0	2	0
Maltese *et al*. [24]	Lateral sled padded High vel.	W9304	1	75	F	64	0	2	0
Maltese *et al*. [24]	Lateral sled padded low vel.	SC136	1	54	F	61	0	0	0
Maltese *et al*. [24]	Lateral sled padded low vel.	SC115	1	72	M	66	0	0	0
Maltese *et al*. [24]	Lateral sled padded low vel.	SC138	1	58	F	64	0	0	0

TABLE AIV

PMHS OVERVIEW AND APPLIED DATA CENSORING

Note on censoring status: 0: Right censored data, 2: Left censored data, 3: interval censored data

Maltese *et al*. [24]	Lateral sled rigid High vel.	SC108	1	44	M	83	0	0	0
Maltese *et al*. [24]	Lateral sled rigid High vel.	SC109	1	49	F	62	0	0	0
Maltese *et al*. [24]	Lateral sled rigid High vel.	W9310	1	68	M	98	2	2	0
Maltese *et al*. [24]	Lateral sled rigid High vel.	W9301	1	63	M	61	0	2	0
Maltese *et al*. [24]	Lateral sled rigid High vel.	W9302	1	77	M	75	2	2	0
Maltese *et al*. [24]	Lateral sled rigid High vel.	W9309	1	73	F	51	0	0	0
Maltese *et al*. [24]	Lateral sled rigid High vel.	94LSI32R05	1	73	M	72	2	0	0
Maltese *et al*. [24]	Lateral sled rigid High vel.	W9313	1	72	M	73	0	0	0
Maltese *et al*. [24]	Lateral sled rigid High vel.	W9308	1	74	F	65	2	2	0
Maltese *et al*. [24]	Lateral sled rigid pelvis offset	SC113	1	74	M	61	0	0	0
Maltese *et al*. [24]	Lateral sled rigid low vel.	SAC102	1	51	F	63	0	0	0
Maltese *et al*. [24]	Lateral sled rigid low vel.	SC124	1	45	F	64	0	0	0
Maltese *et al*. [24]	Lateral sled rigid low vel.	SC135	1	56	M	72	0	0	0
Maltese *et al*. [24]	Lateral sled rigid low vel.	SC102	1	27	M	89	0	0	0
Maltese *et al*. [24]	Lateral sled rigid low vel.	SC101	1	73	F	65	0	0	0
Maltese *et al*. [24]	Lateral sled rigid low vel.	SIC-08	1	64	NA	73	2	2	0
Maltese *et al*. [24]	Lateral sled rigid low vel.	SC120	1	67	F	74	0	0	0
Maltese *et al*. [24]	Lateral sled rigid low vel.	SC121	1	86	M	67	0	0	0
Maltese *et al*. [24]	Lateral sled rigid low vel.	SC137	1	73	F	64	0	0	0
Maltese *et al*. [24]	Lat. sled rigid abdominal offset	SC125	1	68	M	81	0	0	0
Maltese *et al*. [24]	Lat. sled rigid abdominal offset	SC129	1	51	F	65	0	0	0
Maltese *et al*. [24]	Lateral sled rigid thorax offset	SC128	1	46	F	69	0	0	0
Maltese *et al*. [24]	Lateral sled rigid thorax offset	SC130	1	39	M	66	0	0	0
Maltese *et al*. [24]	Lateral sled rigid thorax offset	SC141	1	79	M	74	0	0	0
Maltese *et al*. [24]	Lateral sled rigid thorax offset	SC142	1	58	F	48	0	0	0
Nusholtz *et al*. [14]	Steering-wheel impactor	86M060	2	61	M	61	3	0	0
Nusholtz *et al*. [14]	Steering-wheel impactor	86M040	7	46	M	50	3	0	0
Nusholtz *et al*. [14]	Steering-wheel impactor	86M050	4	55	F	70	0	0	0

TABLE AV

EXPERIMENTAL TESTS AND IRFS METRIC VALUES OVERVIEW

Grey lines correspond to the experiments which were not replicated. The metric values were deduced from regression.

Configuration	Test Number	PMHS Number	Liver MPS95	Spleen MPS95	SI Press95 (MPA)
Hardy *et al*. [13] Bar impact 48 kg T11	GI10	28800	0.7455	0.572	0.221
Hardy *et al.* [13] Bar impact 48 kg T11	GI11	29115	0.6166	0.428	0.139
Hardy *et al.* [13] Bar impact 48 kg T11	GI5	29084	0.6239	0.437	0.144
Cavanaugh *et al*. [15] Bar impact 31 kg L3	24	525	0.3305	0.284	0.175
Cavanaugh *et al*. [15] Bar impact 31 kg L3	19	473	0.3285	0.278	0.169
Cavanaugh *et al*. [15] Bar impact 31 kg L3	33	590	0.3821	0.357	0.212
Cavanaugh *et al*. [15] Bar impact 31 kg L3	37	684	0.5105	0.451	0.266
Cavanaugh *et al*. [15] Bar impact 31 kg L3	61	786	0.5735	0.483	0.293
Cavanaugh *et al*. [15] Bar impact 31 kg L3	57	751	0.6125	0.499	0.307
Cavanaugh *et al*. [15] Bar impact 31 kg L3	28	578	0.3628	0.328	0.194
Cavanaugh *et al*. [15] Bar impact 63 kg L3	45	731	0.528	0.454	0.262
Cavanaugh *et al*. [15] Bar impact 63 kg L3	47	739	0.601	0.521	0.287
Cavanaugh *et al*. [15] Bar impact 63 kg L3	43	721	0.529	0.455	0.262
Cavanaugh *et al*. [15] Bar impact 63 kg L1	41	712	0.674	0.614	0.251
Hardy *et al*. [13] Airbag-like impact	AS3	29490	0.163	0.0738	0.158
Hardy *et al*. [13] Airbag-like impact	AS5	29566	0.188	0.0955	0.205
Hardy *et al*. [13] Airbag-like impact	AS2	29490	0.182	0.0907	0.195
Hardy *et al*. [13] Airbag-like impact	AS6	29491	0.164	0.0747	0.161
Viano *et al*. [20] Left Lateral impact Xiphoid	2	863	0.478	0.589	0.101
Viano *et al*. [20] Left Lateral impact Xiphoid	3	RNY1	0.548	0.663	0.124
Viano *et al.* [20] Left Oblique impact Xiphoid	17	986	0.426	0.449	0.133
Viano *et al.* [20] Left Oblique impact Xiphoid	33	063	0.577	0.566	0.255
Viano *et al.* [20] Left Oblique impact Xiphoid	4	935	0.442	0.458	0.145
Viano *et al.* [20] Left Oblique impact Xiphoid	37	UOM1	0.569	0.557	0.239
Viano *et al*. [20] Left Oblique impact Xiphoid	7	954	0.487	0.491	0.172
Viano *et al.* [20] Left Oblique impact Xiphoid	14	993	0.516	0.516	0.196
Viano *et al*. [20] Left Oblique impact Xiphoid	5	947	0.483	0.489	0.167
Viano *et al*. [20] Left Oblique impact Xiphoid	9	RNY2	0.483	0.489	0.168
Viano *et al*. [20] Left Oblique impact Xiphoid	11	956	0.463	0.474	0.156
Viano *et al*. [20] Right Oblique impact Xiphoid	29	008	0.554	0.185	0.116
Viano *et al*. [20] Right Oblique impact Xiphoid	36	UOM1	0.455	0.129	0.085
Viano *et al*. [20] Left Oblique impact Abdomen	42	UOM2	0.220	0.347	0.153
Viano *et al*. [20] Left Oblique impact Abdomen	30	008	0.322	0.468	0.216
Viano *et al.* [20] Left Oblique impact Abdomen	20	986	0.300	0.590	0.368
Viano *et al*. [20] Right Oblique impact Abdomen	28	047	0.624	0.313	0.231

TABLE AV

EXPERIMENTAL TESTS AND IRFS METRIC VALUES OVERVIEW

Grey lines correspond to the experiments which were not replicated. The metric values were deduced from regression.

Configuration	Test Number	PMHS Number	Liver MPS95	Spleen MPS95	SI Press95 (MPA)
Viano *et al*. [20] Right Oblique impact Abdomen	43	UOM2	0.398	0.103	0.105
Viano *et al*. [20] Right Oblique impact Abdomen	12	956	0.541	0.231	0.172
Viano *et al*. [20] Right Oblique impact Abdomen	6	947	0.573	0.250	0.188
Viano *et al*. [20] Right Oblique impact Abdomen	8	954	0.571	0.247	0.186
Viano *et al*. [20] Right Oblique impact Abdomen	10	RNY2	0.567	0.240	0.181
Viano *et al*. [20] Right Oblique impact Abdomen	18	986	0.633	0.313	0.231
Viano *et al*. [20] Right Oblique impact Abdomen	15	993	0.595	0.275	0.204
Viano *et al*. [20] Right Oblique impact Abdomen	34	063	0.654	0.363	0.278
Foster *et al*. [18] Lap-Belt loading	A-1	31658	0.561	0.492	0.563
Foster *et al*. [18] Lap-Belt loading	A-2	31996	0.554	0.489	0.542
Foster *et al*. [18] Lap-Belt loading	A-3	750	0.590	0.505	0.650
Foster *et al*. [18] Lap-Belt loading	A-4	32016	0.583	0.502	0.628
Foster *et al*. [18] Lap-Belt loading	B-1	31719	0.485	0.360	0.405
Foster *et al*. [18] Lap-Belt loading	B-2	623	0.477	0.368	0.382
Foster *et al*. [18] Lap-Belt loading	B-3	694	0.504	0.399	0.420
Foster *et al*. [18] Lap-Belt loading	C-1	31860	0.212	0.166	0.137
Lamielle *et al.* [17] Lap-Belt loading	MHA111	MS586	0.344	0.397	0.315
Lamielle *et al.* [17] Lap-Belt loading	MHA115	MS587	0.330	0.384	0.294
Lamielle *et al.* [17] Lap-Belt loading	MHA151	MS588	0.367	0.378	0.321
Lamielle *et al.* [17] Lap-Belt loading	MHA155	MS589	0.335	0.399	0.333
Lamielle *et al.* [17] Lap-Belt loading	PRT052	MS580	0.514	0.373	0.435
Lamielle *et al.* [17] Lap-Belt loading	PRT053	MS581	0.510	0.371	0.430
Lamielle *et al.* [17] Lap-Belt loading	PRT065	MS582	0.461	0.328	0.365
Lamielle *et al.* [17] Lap-Belt loading	PRT066	MS583	0.442	0.314	0.340
Hardy *et al*. [13] Lap-Belt loading	CB1	29311	0.391	0.315	0.353
Hardy *et al*. [13] Lap-Belt loading	CB3	29116	0.386	0.324	0.319
Hardy *et al*. [13] Lap-Belt loading	CB5	29131	0.391	0.343	0.328
Ramachandra *et al.* [5] Lap-Belt loading	1	na	0.373	0.272	0.283
Ramachandra *et al.* [5] Lap-Belt loading	2	na	0.363	0.272	0.288
Ramachandra *et al.* [5] Lap-Belt loading	3	na	0.367	0.268	0.291
Ramachandra *et al*. [5] Lap-Belt loading	04_1	na	0.340	0.254	0.285
Ramachandra *et al*. [5] Lap-Belt loading	6	na	0.354	0.252	0.292
Ramachandra *et al*. [5] Lap-Belt loading	07_2	na	0.395	0.298	0.344
Ramachandra *et al*. [5] Lap-Belt loading	04_2	na	0.368	0.284	0.306
Ramachandra *et al*. [5] Lap-Belt loading	5_1	na	0.419	0.305	0.335
Ramachandra *et al*. [5] Lap-Belt loading	05_2	na	0.366	0.283	0.305
Ramachandra *et al*. [5] Lap-Belt loading	07_1	na	0.383	0.290	0.315
Trosseille *et al*. [16] Lap-Belt loading	PRT037	MS515	0.556	0.485	0.533
Trosseille *et al.* [16] Lap-Belt loading	PRT038	MS517	0.610	0.487	0.654
Trosseille *et al*. [16] Lap-Belt loading	PRT039	MS520	0.594	0.456	0.6064
Trosseille *et al*. [16] Lap-Belt loading	PRT034	MS503	0.556	0.485	0.533
Trosseille *et al*. [16] Lap-Belt loading	PRT035	MS505	0.556	0.485	0.533
Trosseille *et al.* [16] Lap-Belt loading	PRT036	MS507	0.556	0.485	0.533
Kremer *et al*. [21] Right lateral impact	FBL03-L	na	0.521	0.245	0.111
Kremer *et al*. [21] Right lateral impact	FBL11-L	na	0.539	0.272	0.124
Kremer *et al*. [21] Right lateral impact	FBL01-L	na	0.530	0.259	0.117
Kremer *et al*. [21] Right lateral impact	FBL02-L	na	0.534	0.266	0.121
Kremer *et al*. [21] Right lateral impact	FBL04-L	na	0.531	0.260	0.118
Kremer *et al*. [21] Right oblique impact	FBL05-O	na	0.518	0.232	0.131
Kremer *et al*. [21] Right oblique impact	FBL06-O	na	0.539	0.270	0.153
Kremer *et al*. [21] Right oblique impact	FBL07-O	na	0.537	0.266	0.151
Kremer *et al*. [21] Right oblique impact	FBL08-O	na	0.530	0.253	0.144
Kremer *et al*. [21] Right oblique impact	FBL09-O	na	0.538	0.268	0.152
Walfish *et al.* [22] Lateral drop test	205	na	0.517	0.197	0.079
Walfish *et al.* [22] Lateral drop test	206	na	0.596	0.276	0.118
Walfish *et al.* [22] Lateral drop test	215	na	0.675	0.331	0.144
Walfish *et al.* [22] Lateral drop test	217	na	0.639	0.279	0.150
Hardy *et al.* [13] Bar impact 48 kg L3	GI6	28838	0.339	0.306	0.177
Hardy *et al*. [13] Bar impact 48 kg L3	GI4	28764	0.393	0.366	0.215
Hardy *et al.* [13] Bar impact 48 kg L3	GI9	28942	0.586	0.507	0.285
Hardy *et al.* [13] Bar impact 48 kg L3	GI3	28682	0.363	0.333	0.194
Hardy *et al*. [13] Bar impact 48 kg L3	GI8	28889	0.517	0.458	0.259
Hardy *et al*. [13] Bar impact 48 kg L3	GI7	28879	0.495	0.441	0.251
Howes *et al*. [19] 3-pt belt loading	SM101	na	0.649	0.470	0.342
Howes *et al.* [19] 3-pt belt loading	SM102	na	0.652	0.489	0.360
Howes *et al*. [19] 3-pt belt loading	SM103	na	0.692	0.548	0.414
Howes *et al*. [19] 3-pt belt loading	SM104	na	0.586	0.441	0.329
Howes *et al*. [19] 3-pt belt loading	SM106	na	0.630	0.476	0.362
Howes *et al*. [19] 3-pt belt loading	SM108	na	0.625	0.505	0.377
Cavanaugh *et al*. [23] Lat. Sled 102 mm stiff padding	SIC09	na	0.499	0.602	0.337
Cavanaugh *et al*. [23] Lat. Sled 102 mm stiff padding	SIC12	na	0.499	0.602	0.337
Cavanaugh *et al*. [23] Lat. Sled 102 mm stiff padding	SIC14	na	0.499	0.602	0.337
Cavanaugh *et al*. [23] Lat. Sled 102 mm stiff padding	SIC16	na	0.499	0.602	0.337
Cavanaugh *et al*. [23] Lat. Sled 102 mm soft padding	SIC13	na	0.494	0.569	0.337
Cavanaugh *et al*. [23] Lat. Sled 102 mm soft padding	SIC15	na	0.494	0.569	0.337
Cavanaugh *et al*. [23] Lat. Sled 152 mm soft padding	SIC10	na	0.483	0.565	0.304
Cavanaugh *et al*. [23] Lat. Sled 152 mm soft padding	SIC11	na	0.483	0.565	0.304
Cavanaugh *et al*. [23] Lat. Sled 152 mm soft padding	SIC17	na	0.483	0.565	0.304
Cavanaugh *et al.* [23] Lat. Sled Rigid_wall	SIC05	na	0.443	0.506	0.268
Cavanaugh *et al.* [23] Lat. Sled Rigid_wall	SIC07	na	0.443	0.506	0.268

TABLE AV

EXPERIMENTAL TESTS AND IRFS METRIC VALUES OVERVIEW

Grey lines correspond to the experiments which were not replicated. The metric values were deduced from regression.

Configuration	Test Number	PMHS Number	Liver MPS95	Spleen MPS95	SI Press95 (MPA)
Cavanaugh *et al.* [23] Lat. Sled Rigid_wall	SIC08	na	0.443	0.506	0.268
Cavanaugh *et al.* [23] Lat. Sled Rigid_wall	SIC04	na	0.530	0.636	0.392
Cavanaugh *et al.* [23] Lat. Sled Rigid_wall	SIC06	na	0.530	0.636	0.392
Maltese *et al*. [24] Lateral sled padded High vel.	5243	SC134	0.502	0.567	0.345
Maltese *et al*. [24] Lateral sled padded High vel.	3278	SC107	0.502	0.567	0.345
Maltese *et al*. [24] Lateral sled padded High vel.	3323	W9303	0.502	0.567	0.345
Maltese *et al*. [24] Lateral sled padded High vel.	3320	W9306	0.502	0.567	0.345
Maltese *et al*. [24] Lateral sled padded High vel.	3581	W9312	0.502	0.567	0.345
Maltese *et al*. [24] Lateral sled padded High vel.	5242	SC133	0.502	0.567	0.345
Maltese *et al*. [24] Lateral sled padded High vel.	3589	SC116	0.502	0.567	0.345
Maltese *et al*. [24] Lateral sled padded High vel.	3586	W9314	0.502	0.567	0.345
Maltese *et al*. [24] Lateral sled padded High vel.	3935	LSI32P15	0.502	0.567	0.345
Maltese *et al*. [24] Lateral sled padded High vel.	3936	LSI32P16	0.502	0.567	0.345
Maltese *et al*. [24] Lateral sled padded High vel.	3321	W9304	0.502	0.567	0.345
Maltese *et al*. [24] Lateral sled padded Low vel.	5470	SC136	0.429	0.455	0.242
Maltese *et al*. [24] Lateral sled padded Low vel.	3588	SC115	0.429	0.455	0.242
Maltese *et al*. [24] Lateral sled padded Low vel.	5472	SC138	0.429	0.455	0.242
Maltese *et al*. [24] Lateral sled rigid High vel.	3422	SC108	0.545	0.627	0.357
Maltese *et al*. [24] Lateral sled rigid High vel.	3423	SC109	0.545	0.627	0.357
Maltese *et al*. [24] Lateral sled rigid High vel.	3579	W9310	0.545	0.627	0.357
Maltese *et al*. [24] Lateral sled rigid High vel.	3325	W9301	0.545	0.627	0.357
Maltese *et al*. [24] Lateral sled rigid High vel.	3324	W9302	0.545	0.627	0.357
Maltese *et al*. [24] Lateral sled rigid High vel.	3578	W9309	0.545	0.627	0.357
Maltese *et al.* [24] Lateral sled rigid High vel.	3322	94LSI32R05	0.545	0.627	0.357
Maltese *et al.* [24] Lateral sled rigid High vel.	3585	W9313	0.545	0.627	0.357
Maltese *et al.* [24] Lateral sled rigid High vel.	3577	W9308	0.545	0.627	0.357
Maltese *et al*. [24] Lateral sled rigid pelvis offset	3538	SC113	0.174	0.451	0.266
Maltese *et al*. [24] Lateral sled rigid Low vel.	4348	SAC102	0.461	0.491	0.260
Maltese *et al*. [24] Lateral sled rigid Low vel.	4340	SC124	0.461	0.491	0.260
Maltese *et al*. [24] Lateral sled rigid Low vel.	5244	SC135	0.461	0.491	0.260
Maltese *et al*. [24] Lateral sled rigid Low vel.	3122	SC102	0.461	0.491	0.260
Maltese *et al*. [24] Lateral sled rigid Low vel.	3120	SC101	0.461	0.491	0.260
Maltese *et al*. [24] Lateral sled rigid Low vel.	5825	SIC-08	0.461	0.491	0.260
Maltese *et al*. [24] Lateral sled rigid Low vel.	3664	SC120	0.461	0.491	0.260
Maltese *et al*. [24] Lateral sled rigid Low vel.	3700	SC121	0.461	0.491	0.260
Maltese *et al*. [24] Lateral sled rigid Low vel.	5471	SC137	0.461	0.491	0.260
Maltese *et al*. [24] Lat. sled rigid abdominal offset	4218	SC125	0.476	0.443	0.240
Maltese *et al*. [24] Lat. sled rigid abdominal offset	4295	SC129	0.476	0.443	0.245
Maltese *et al.* [24] Lat. sled rigid thoracic offset	4338	SC128	0.476	0.544	0.245
Maltese *et al*. [24] Lat. sled rigid thoracic offset	4296	SC130	0.476	0.544	0.245
Maltese *et al*. [24] Lat. sled rigid thoracic offset	7584	SC141	0.476	0.544	0.245
Maltese *et al*. [24] Lat. sled rigid thoracic offset	7831	SC142	0.476	0.544	0.245
Nusholtz *et al.* [14] "Steering wheel" impact abdomen	Preliminary test 86m060	86M060	0.179	0.083	0.086
Nusholtz *et al.* [14] "Steering wheel" impact abdomen	Preliminary test 86m040	86M040	0.250	0.149	0.122
Nusholtz *et al*. [14] "Steering wheel" impact sternum	Injurious test 86m060	86M060	0.404	0.220	0.061
Nusholtz *et al*. [14] "Steering wheel" impact abdomen	Injurious test 86m040	86M040	0.552	0.590	0.366
Nusholtz *et al*. [14] "Steering wheel" impact abdomen	Injurious test 86m050	86M050	0.499	0.524	0.316

TABLE AVI

EXCLUDED TESTS AND STUDY

Ref.	PMHS Number	Reason for exclusion
[22]	216	authors have observed pre-existing abnormalities of the liver
[22]	219	authors have observed pre-existing abnormalities of the liver
[22]	209	Non-rigid armrest: unknown material properties
[22]	210	Non-rigid armrest: unknown material properties
[22]	211	Non-rigid armrest: unknown material properties
[22]	212	Non-rigid armrest: unknown material properties
[22]	213	Non-rigid armrest: unknown material properties
[14]	86M001	Two impacted sites: lower sternum or rib 10 contact region. It cannot be told to what configuration is due the abdominal injury (Liver, right kidney).
[14]	86M010	Two impacted sites. Hypothesis: abdominal injury (Vena cava, liver, stomach) could be attributed to below sternum impact configurations: 9 repeated tests at 2 m/s.
[14]	86M020	Two impacted sites. Difficult to attribute the abdominal injuries (Liver, Kidney, Jejunum) to a test configuration or another. They are likely due to the below sternum impact configuration (n=8 at ~3 m/s) but some could be attributed to abdomen impact configuration (n=6).
[14]	86M030	Impact at the soft abdomen region only but repeatedly: (n=6 at ~3 m/s; last one at 10.8 m/s) Superficial laceration of superior left lobe of liver. No thoracic injury.
[13]	28594	Injury not available. The was used as proof-of-concept for the newly fabricated test facility
[13]	29311 (test CB2)	Configuration with seatback not simulated. However, this subject was used in test CB1 (without seatback) which was considered as right censored in our analysis (used in group 1 only)
[13]	29116 (test CB4)	Configuration with the belt below the ASIS which was not simulated. However, this subject was used in test CB3 (belt at mid abdomen) which was considered as right censored in our analysis (used in group 1 only)
[13]	29131 (test CB6)	Configuration with the belt below the ASIS which was not simulated. However, this subject was used in test CB6 (belt at mid abdomen) which was considered as right censored in our analysis (used in group 1 only)
[18]	31860 (test C2)	Configuration with the belt on the epigastric region which was not simulated. However, this subject was used in test C1 (belt at mid abdomen) which was considered as right censored in our analysis (used in group 1 only)
[A1]	4	Difficult to reproduce the configuration (validation of the airbag model)
[A1]	5	Difficult to reproduce the configuration (validation of the airbag model)
[A1]	6	Difficult to reproduce the configuration (validation of the airbag model)
[A1]	7	Difficult to reproduce the configuration (validation of the airbag model)

TABLE AVII

SIMULATION AND INTERPOLATED POINTS

Ref.	Liver MPS95 regression	Spleen MPS95 regression	SI 95th Pressure regression
[13]	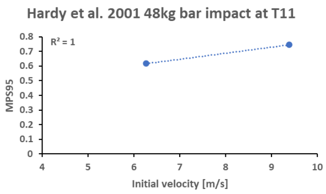	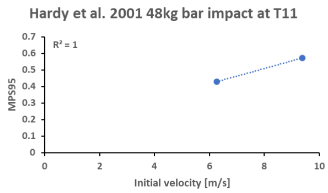	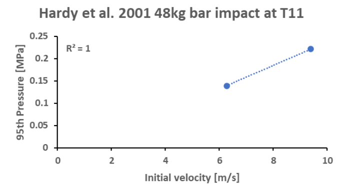
[15]	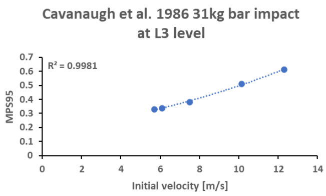	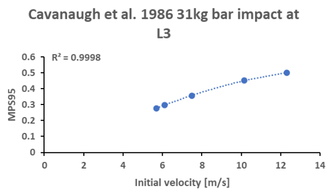	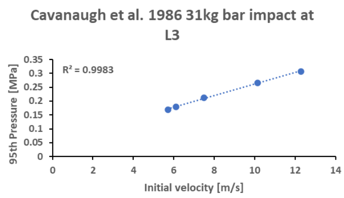
[15]	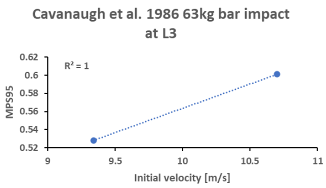	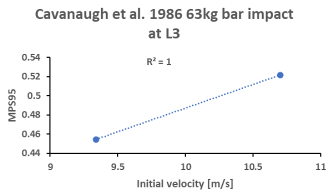	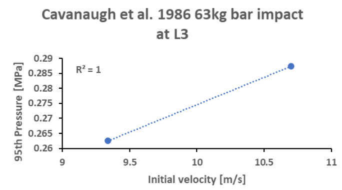
[5]	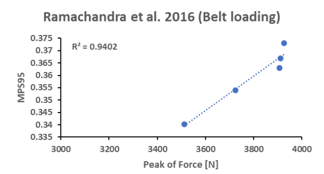	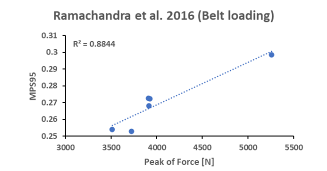	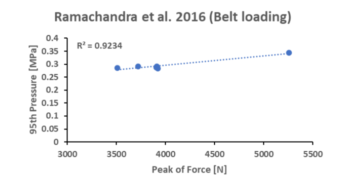
[13]	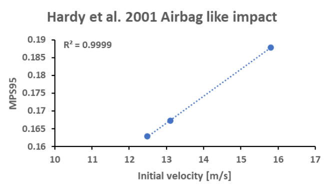	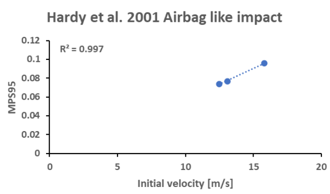	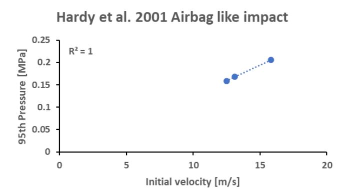
[20]	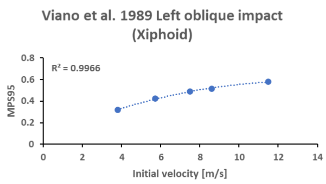	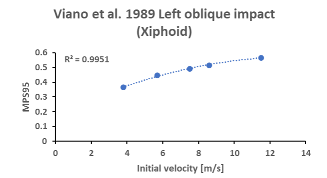	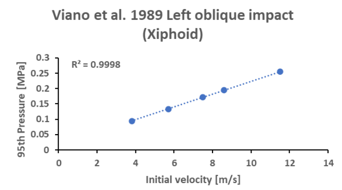
[20]	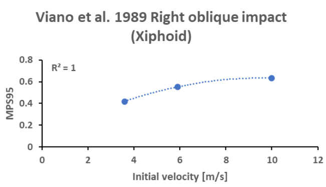	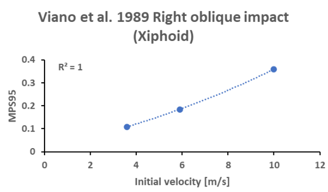	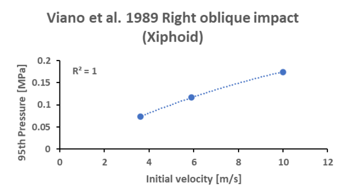
[20]	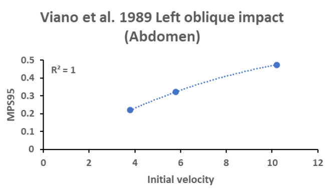	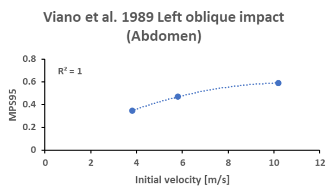	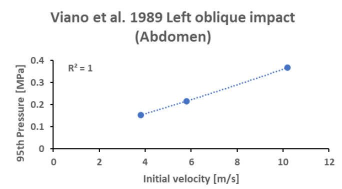
[20]	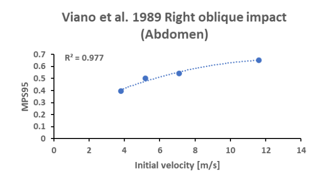	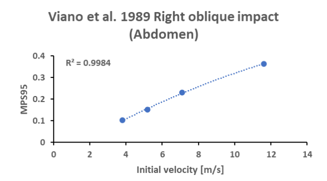	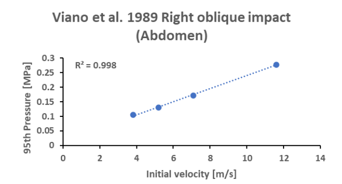

TABLE AVII
SIMULATION AND INTERPOLATED POINTS

Ref.	Liver MPS95 regression	Spleen MPS95 regression	SI 95th Pressure regression
[21]	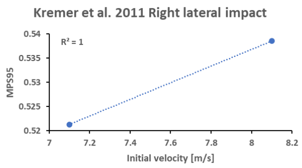	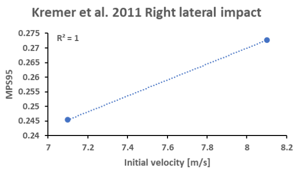	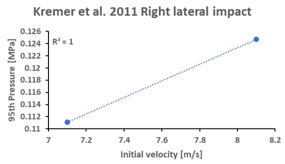
[21]	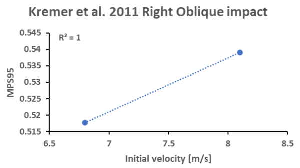	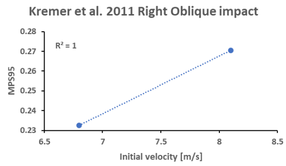	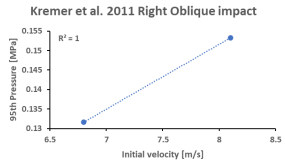
[22]	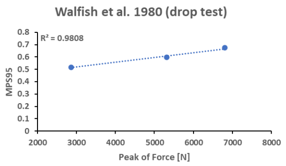	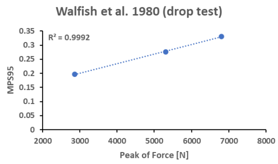	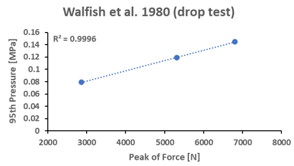
[13]	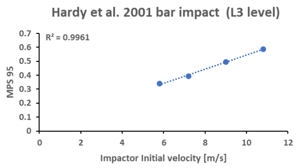	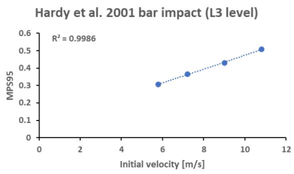	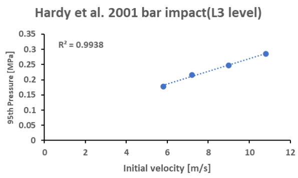

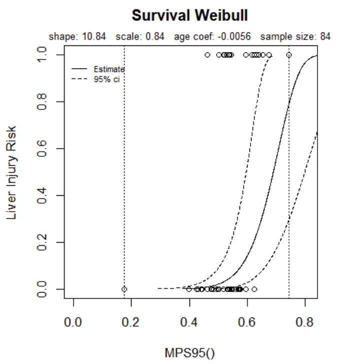

Fig. AI. Liver IRF at 30yrs old (group 2)

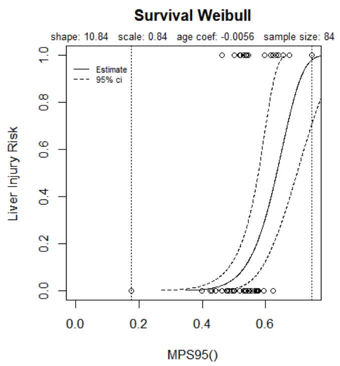

Fig. AII. Liver IRF at 45yrs old (group 2)

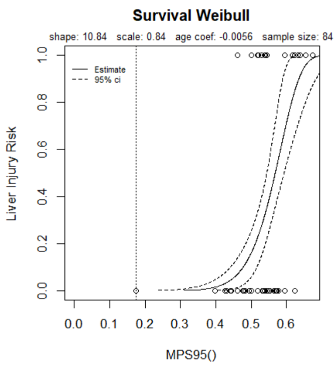

Fig. AIII. Liver IRF at 65yrs old (group 2)

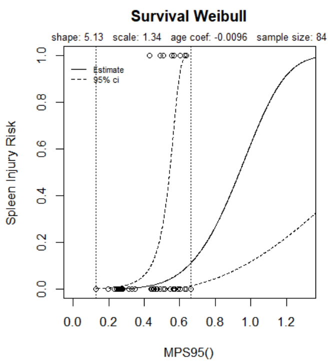

Fig. AIV. Spleen IRF at 30yrs old (group 2)

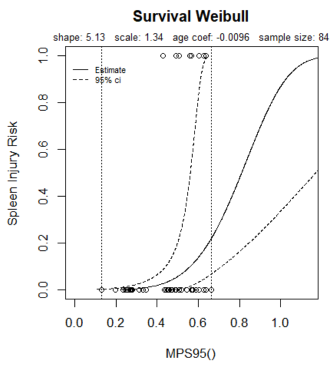

Fig. AV. Spleen IRF at 45yrs old (group 2)

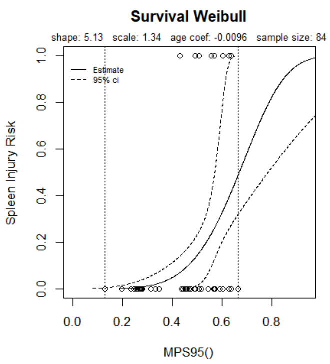

Fig. AVI. Spleen IRF at 65yrs old (group 2)

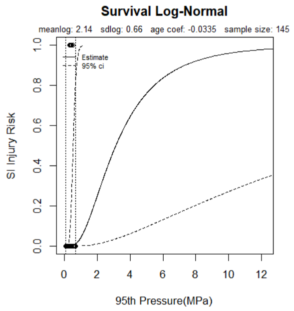

Fig. AVII. SI IRF at 30yrs old (group 1)

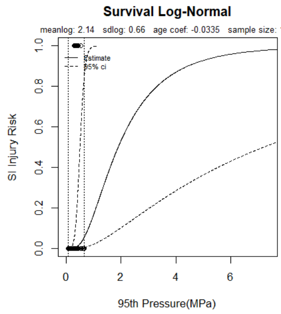

Fig. AVIII. SI IRF at 45yrs old (group 1)

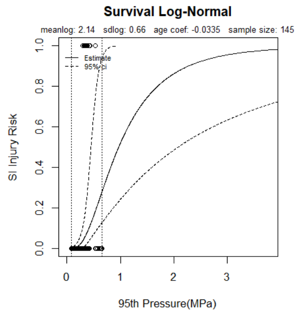

Fig. AIX. SI IRF at 65yrs old (group 1)

IX. APPENDIX REFERENCES

[A1] Hallman, J.J., Yoganandan, N., Pintar, F.A. (2010) Biomechanical and injury response to posterolateral loading from torso side airbags. *Stapp Car Crash Journal*, **54**: pp. 227-57.